Multi-omics analyses reveal that HIV-1 alters CD4$^+$ T cell immunometabolism to fuel virus replication

Haitao Guo[1,2,10], Qi Wang[1,10], Khader Ghneim[3], Li Wang[4], Elena Rampanelli[1], Elizabeth Holley-Guthrie[1,2], Liang Cheng[1], Carolina Garrido[5], David M. Margolis[5], Leigh A. Eller[6,7], Merlin L. Robb[6,7], Rafick-Pierre Sekaly[3], Xian Chen[1,4], Lishan Su[1,8,9] ✉ and Jenny P.-Y. Ting[1,2,9] ✉

Individuals infected with human immunodeficiency virus type-1 (HIV-1) show metabolic alterations of CD4$^+$ T cells through unclear mechanisms with undefined consequences. We analyzed the transcriptome of CD4$^+$ T cells from patients with HIV-1 and revealed that the elevated oxidative phosphorylation (OXPHOS) pathway is associated with poor outcomes. Inhibition of OXPHOS by the US Food and Drug Administration–approved drug metformin, which targets mitochondrial respiratory chain complex-I, suppresses HIV-1 replication in human CD4$^+$ T cells and humanized mice. In patients, HIV-1 peak viremia positively correlates with the expression of NLRX1, a mitochondrial innate immune receptor. Quantitative proteomics and metabolic analyses reveal that NLRX1 enhances OXPHOS and glycolysis during HIV-1-infection of CD4$^+$ T cells to promote viral replication. At the mechanistic level, HIV infection induces the association of NLRX1 with the mitochondrial protein FASTKD5 to promote expression of mitochondrial respiratory complex components. This study uncovers the OXPHOS pathway in CD4$^+$ T cells as a target for HIV-1 therapy.

Although combination antiretroviral therapy (cART) effectively suppresses HIV-1 viremia, approximately 20% of patients fail to achieve CD4$^+$ T cell recovery and exhibit abnormalities of immune functions, which are likely caused by residue HIV-1 replication in certain tissue compartments in part due to virus mutants that support escape from antiviral therapeutics[1,2]. A complementary approach to cART is to target host factors to restrict virus replication and thus reduce virus mutant escape. Immune cell metabolism (immunometabolism) correlates with HIV-1 restriction in elite controllers and is an emerging field for developing new HIV-1 therapies[3].

HIV-1 infection causes upregulated metabolism of glucose, lipid and tryptophan and elevated oxidative stress in immune cells[4]. Among these, glucose metabolism is the most critical to meet energy and biosynthesis needs for both HIV-1 replication and responses of immune cells[5,6], as evident by upregulated expression of glucose transporter 1 (GLUT1), which resulted in increased uptake of glucose in inflammatory monocytes and CD4$^+$ T cells from patients with HIV-1 (refs. [2,7]). The reprogramming of glucose breakdown, glycolysis and oxidative phosphorylation in patients with HIV-1 has been documented[2,4,8]; however, the mechanisms are unknown. Although metabolic alteration has been associated with HIV-1 replication, immune abnormalities and disease complications, how HIV-1 infection reprograms immunometabolism is unknown. This hinders the development of new HIV-1 disease therapy by targeting metabolism[3].

The nucleotide-binding domain and leucine-rich repeat-containing receptor X1 (NLRX1), a multifunctional innate immune regulator[9–12], contributes to CD4$^+$ T cell polarization and proliferation. NLRX1 also regulates mitochondrial reactive oxygen species production, suggesting a potential role in metabolism[13]. Notably, the role of NLRX1 in facilitating HIV-1 replication has been demonstrated in myeloid cells[14]; furthermore, NLRX1 expression in nonhuman primates is positively correlated with simian immunodeficiency virus viremia[15]. However, whether and how NLRX1 plays a role in HIV-1 replication in CD4$^+$ T cells, the major cell type that produces HIV-1 in vivo, remains unstudied and unknown.

This study used transcriptomic and proteomic analyses to reveal that an enhancement of OXPHOS is associated with HIV-1 infection and disease progression. Repurposing the US Food and Drug Administration (FDA)-approved agent metformin, which targets mitochondrial complex-I and therefore OXPHOS, suppresses HIV-1 replication in both primary CD4$^+$ T cell cultures and humanized mice. Mechanistically, NLRX1 interacts with another mitochondrial protein, FAST kinase domain-containing protein 5 (FASTDK5) and cooperatively promotes both OXPHOS and HIV-1 replication in CD4$^+$ T cells. These results raise the promise of controlling HIV-1 replication by targeting the NLRX1–OXPHOS axis.

Results

HIV-1 viral load set point in patients positively correlates with oxidative phosphorylation. Immunometabolism is dysregulated

[1]Lineberger Comprehensive Cancer Center, University of North Carolina at Chapel Hill, Chapel Hill, NC, USA. [2]Department of Genetics, University of North Carolina at Chapel Hill, Chapel Hill, NC, USA. [3]Department of Pathology, Emory University, Atlanta, GA, USA. [4]Department of Biochemistry & Biophysics, University of North Carolina at Chapel Hill, Chapel Hill, NC, USA. [5]HIV Cure Center and Department of Medicine, University of North Carolina at Chapel Hill, Chapel Hill, NC, USA. [6]US Military HIV Research Program, Walter Reed Army Institute of Research, Silver Spring, MD, USA. [7]Henry M. Jackson Foundation for the Advancement of Military Medicine, Bethesda, MD, USA. [8]Institute of Human Virology, University of Maryland School of Medicine, Baltimore, MD, USA. [9]Department of Microbiology and Immunology, University of North Carolina at Chapel Hill, Chapel Hill, NC, USA. [10]These authors contributed equally: Haitao Guo, Qi Wang. ✉e-mail: lsu@ihv.umaryland.edu; jenny_ting@med.unc.edu

in patients with HIV-1 and is associated with HIV-1 cellular susceptibility and reactivation in in vitro assays[16–19]. To address how immunometabolic changes contribute to HIV-1 replication, we first analyzed gene expression data from the RV217 transcriptomic study of human subjects acutely infected with HIV-1 in Asia and Africa[20]. Transcriptomes of CD4+ T cells from the Asian (all males, $n=23$) and African (all females, $n=18$) cohort were clustered together regardless of geography (Fig. 1a) and the key prognosis parameter of HIV-1 disease progression, set-point viral load[21], was not significantly different between these two cohorts (Fig. 1b). Linear regression analysis between gene expression and set-point viral load is used to assess how major metabolic pathways of interest are correlated with the magnitude of set-point viral load in sorted CD4+ T cells from individuals infected with HIV-1 in both Asian and African cohorts. We found that the OXPHOS pathway from the KEGG database (C2, Molecular Signatures database) was the most positively correlated pathway with poor outcome (higher set-point viral load). This observation was consistent in the Asian cohort ($P=0.0057$) and the African cohort ($P=0.0063$). Notably, only the OXPHOS pathway was significantly correlated to a poor outcome when pooling both geographical sites ($P=0.0191$) (Fig. 1c and Supplementary Table 1), suggesting that OXPHOS could serve as a prognosis biomarker for AIDS progression regardless of geographic variation. Furthermore, this observation was validated using the OXPHOS pathway from the Hallmark database ($P<0.001$) (Supplementary Table 2). Leading-edge analysis was performed to examine particular genes of a gene set contributing the most to the enrichment (Asian + African cohort; Supplementary Table 1). The coexpression and interaction network of leading-edge genes of the OXPHOS pathway was established to highlight the top genes contributing to enrichment (Fig. 1d and Extended Data Fig. 1). The peak viremia of HIV-1 in acute infection usually predicts viral load at the set point[22]. It is highly likely that the OXPHOS-associated higher set-point viral load is attributed to a higher HIV-1 replication in the acute infection phase. Therefore, it is of interest to assess whether altering metabolic pathways, particularly OXPHOS, can affect HIV replication and hence pathogenesis.

HIV-1 replication is suppressed by targeting metabolic pathways. To assess the importance of OXPHOS in HIV-1 infection, pharmacological inhibitors for OXPHOS, including rotenone and antimycin A, which target mitochondrial complex-I and mitochondrial complex-III respectively, significantly suppressed HIV-1 pseudovirus (the vesicular stomatitis virus envelope glycoprotein (VSV-G)-pseudotyped HIV-1 NL4-3-Luc) replication in the human Jurkat T cell line (Extended Data Fig. 2a). Furthermore, the FDA-approved antidiabetic agent metformin, which has been shown to target mitochondrial complex-I (ref. [23]), suppressed OXPHOS in HIV-1 pseudovirus-infected Jurkat cells (Extended Data Fig. 2b,c) and had a similar suppressive effect on HIV-1 replication compared to rotenone (Extended Data Fig. 2a). These data suggest a critical role of OXPHOS in HIV-1 replication in CD4+ T cells. Combined data from the Asian and African cohort of patients with HIV-1 demonstrate that glycolysis also positively correlates with HIV-1 set-point viremia, although with less significance than OXPHOS (Fig. 1c). Blocking glycolysis with 2-deoxyglucose (2-DG) also significantly suppressed VSV-G-NL4-3-Luc replication in Jurkat cells (Extended Data Fig. 2d), congruent with the previous work[19].

Metformin inhibits HIV-1 replication in both primary CD4+ T cells and humanized mice reconstituted with human CD4+ T cells. We next explored the therapeutic value of HIV-1 replication requiring OXPHOS in more physiologically relevant systems by testing human primary CD4+ T cells in culture and in humanized mice. Human primary CD4+ T cells were infected with HIV-1 clinical isolates 409, 413 and 414. Metformin suppressed the replication of all three clinical isolates to a similar extent as rotenone and antimycin A, as measured by intracellular HIV-1 RNA and virion production (Fig. 2a,b). 2-DG offered the best effectiveness in inhibiting HIV-1 replication, likely due to its suppression of both glycolysis and OXPHOS (Fig. 2a,b).

To test the impact of these treatments in vivo in human cells, we used a human CD4+ T cell-reconstituted NOD-*Rag1*^{null} *IL2rg*^{null} (NRG) mouse model (hereafter referred to as NRG-hu CD4+ mice), which supports HIV-1 replication and pathogenesis in vivo[24]. NRG-hu CD4+ mice were infected with the CCR5/CXCR4 dual-tropic HIV-1 strain R3A. One day before infection, half of the NRG-hu CD4+ mice were given metformin in drinking water, while the other half were left untreated. The dose of metformin delivered in vivo was based on the literature to assure minimal toxicity[23,25]. At 2 weeks post-infection (wpi), HIV-1 titer in the metformin-treated group was approximately one order of magnitude lower than that of the untreated control group (Fig. 2c). The depletion of CD4+ T cells is the hallmark of HIV-1 pathogenesis and HIV-1-induced immunodeficiency in patients[26]. Metformin did not alter human CD4+ T cell numbers in peripheral blood at 1 wpi when HIV-1-induced CD4+ T cell depletion had not begun. The drug partially protected human CD4+ T cells from depletion at 2 wpi compared to untreated but HIV-1-infected mice as we observed more 7AAD negative CD4+ T cells in metformin-treated mice (Fig. 2d and Extended Data Fig. 2e). In addition, human CD4+ T cell depletion by HIV in the spleen of NRG-hu CD4+ mice treated with metformin was partially protected (Fig. 2e). As metformin is routinely and safely used for treating diabetes[27] these results suggest that repurposing this drug has the potential to supplement cART for better containment of HIV-1.

NLRX1 positively correlates with both HIV-1 viremia and OXPHOS of CD4+ T cells in patients. We next explored the molecular pathway by which HIV-1 can dynamically regulate OXPHOS to favor its own replication in CD4+ T cells. When we screened the individual gene product correlated with HIV-1 viremia in the RV217 cohort, the mitochondrial protein NLRX1 drew our attention. *NLRX1* transcript levels in CD4+ T cells positively correlated with peak HIV-1 viremia in the RV217 cohort (all males, $n=22$) (Fig. 3a). To confirm this observation, we examined the expression level of *NLRX1* in HIV-1 infected CD4+ T cells in vitro. Staining of endogenous NLRX1 followed by imaging flow cytometry (Extended Data Fig. 3a) showed that NLRX1 protein level was enhanced in Jurkat cells infected with an HIV-1 pseudovirus that expressed green fluorescent protein (GFP) (VSV-G-NL4-3-EGFP) compared to uninfected cells in the same culture (Extended Data Fig. 3b). The expression level of *NLRX1* was positively correlated with HIV-1 replication represented by GFP expression (Extended Data Fig. 3c), which is congruent with the analysis of the RV217 cohort. *NLRX1* messenger RNA was also significantly upregulated in Jurkat cells infected with VSV-G-NL4-3-EGFP (Extended Data Fig. 3d). To provide a more physiological context, we found that *NLRX1* mRNA was increased in human primary CD4+ T cells infected with any one of three different HIV-1 clinical isolates (Extended Data Fig. 3e). NLRX1 is located in the mitochondria, which leads us to hypothesize that NLRX1 may regulate OXPHOS during HIV-1 infection of CD4+ T cells and thus influence viral replication. In fact, we found that in CD4+ T cells sorted from the RV217 cohort, genes whose expression positively correlate with *NLRX1* expression level were significantly enriched in the OXPHOS pathway regardless of the geographic differences (Fig. 3b and Supplementary Table 3). The expression of leading-edge genes in individuals infected with HIV-1 contributing to this enrichment was represented in a heat map along with *NLRX1* expression (Fig. 3c and Supplementary Table 3). These data led us to investigate whether NLRX1 regulates HIV-1-induced oxidative phosphorylation to alter viral replication.

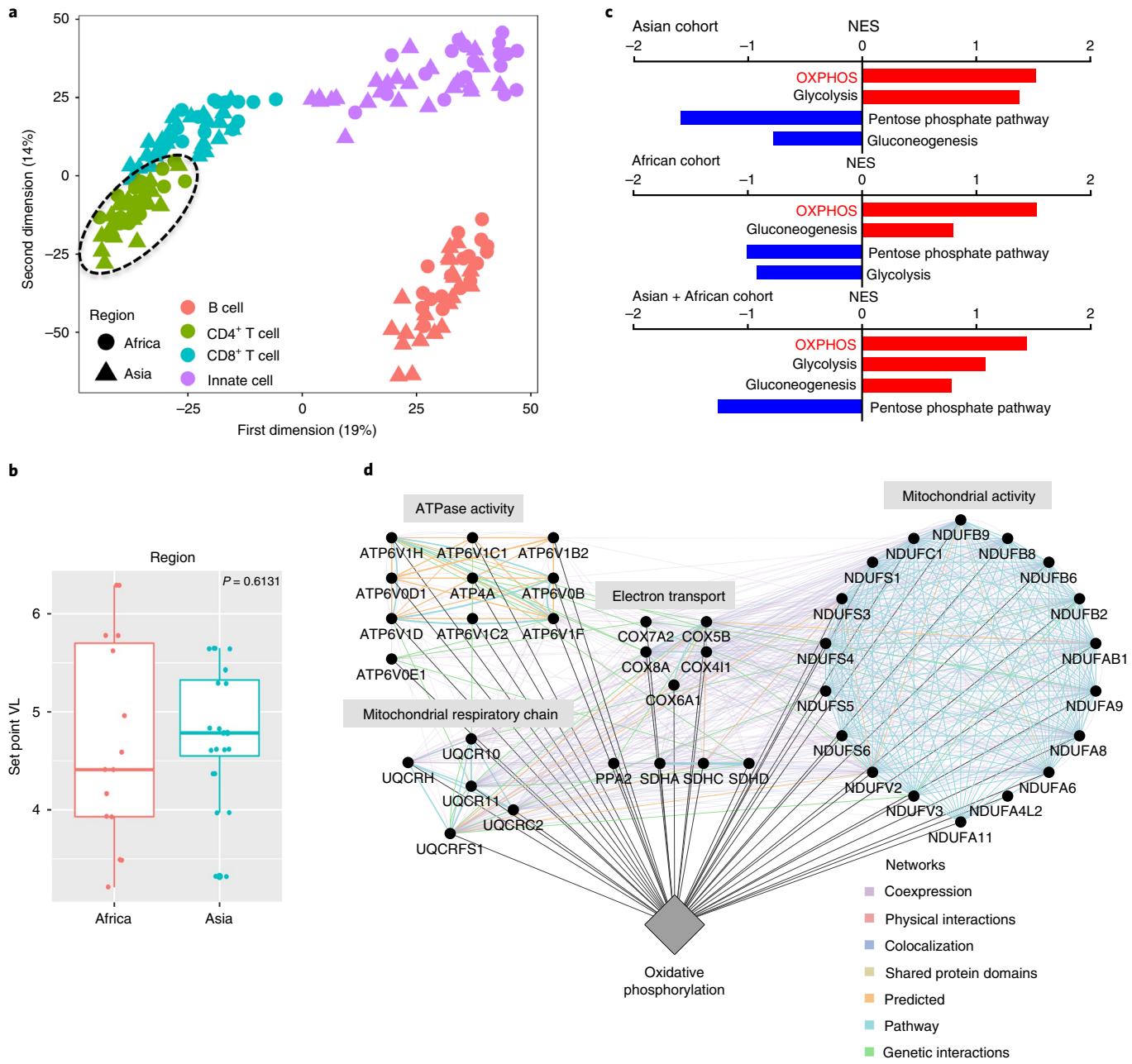

Fig. 1 | Transcriptome analysis of CD4⁺ T cells from patients with HIV-1. a, Multi-dimensional scaling highlighting transcriptomic variance of the full cell-sorted RV217 dataset. Euclidean distance was used. Circle, African cohort; triangle, Asian cohort; red, B cells; green, CD4⁺ T cells; blue, CD8⁺ T cells; and purple, innate cells. **b**, Set-point viral load (VL) was not significantly different between Asian and African RV217 cohorts. Africa, $n = 18$, minima = 3.21, maxima = 6.29; Asia, $n = 22$, minima = 4.61, maxima = 5.65. Jitter-plot displays the first (bottom) and third quartiles (top), the median (line inside box) and 1.5 × interquartile range of upper or lower quartile (whiskers). Significance was assessed by Wilcoxon rank-sum test (one-tailed). **c**, Linear regression analysis between gene expression and set-point VL. Normalized enrichment score (NES) reflects the degree to which a set of genes is overrepresented among genes that are differentially expressed. Bar plot represents positively (red) and negatively (blue) correlated pathways. Supplementary Table 1 provides statistical results for enrichment of these pathways. **d**, The highlight of leading-edge genes of the OXPHOS pathway, which are associated with set-point VL. Circular nodes represent genes, and edges reflect the association between these features. Color of the edge highlights the association between nodes. Biological annotation (diamond nodes) reflecting the function of sets of genes is represented; subfunctions within the network are labeled above groups of genes.

NLRX1 is required for HIV-induced oxidative phosphorylation. To further test the connection between NLRX1 and metabolism alteration during HIV-1 replication in CD4⁺ T cells, we diminished NLRX1 expression in the human Jurkat T cell line by two short hairpin (sh)RNA (sh-NLRX1 line 1 and line 2) and profiled the proteome of VSV-G-NL4-3-Luc-infected and uninfected Jurkat cells by quantitative mass spectrometry. We normalized protein levels in VSV-G-NL4-3-Luc-infected cells containing two individual sh-NLRX1 (Jurkat-sh-NLRX1 line 1 and line 2) and cells containing a control shRNA (Jurkat-sh-Ctr) by protein levels in uninfected cells. Compared to Jurkat-sh-Ctr cells, 336 proteins in Jurkat-sh-NLRX1 line 1 and 294 proteins in Jurkat-sh-NLRX1 line

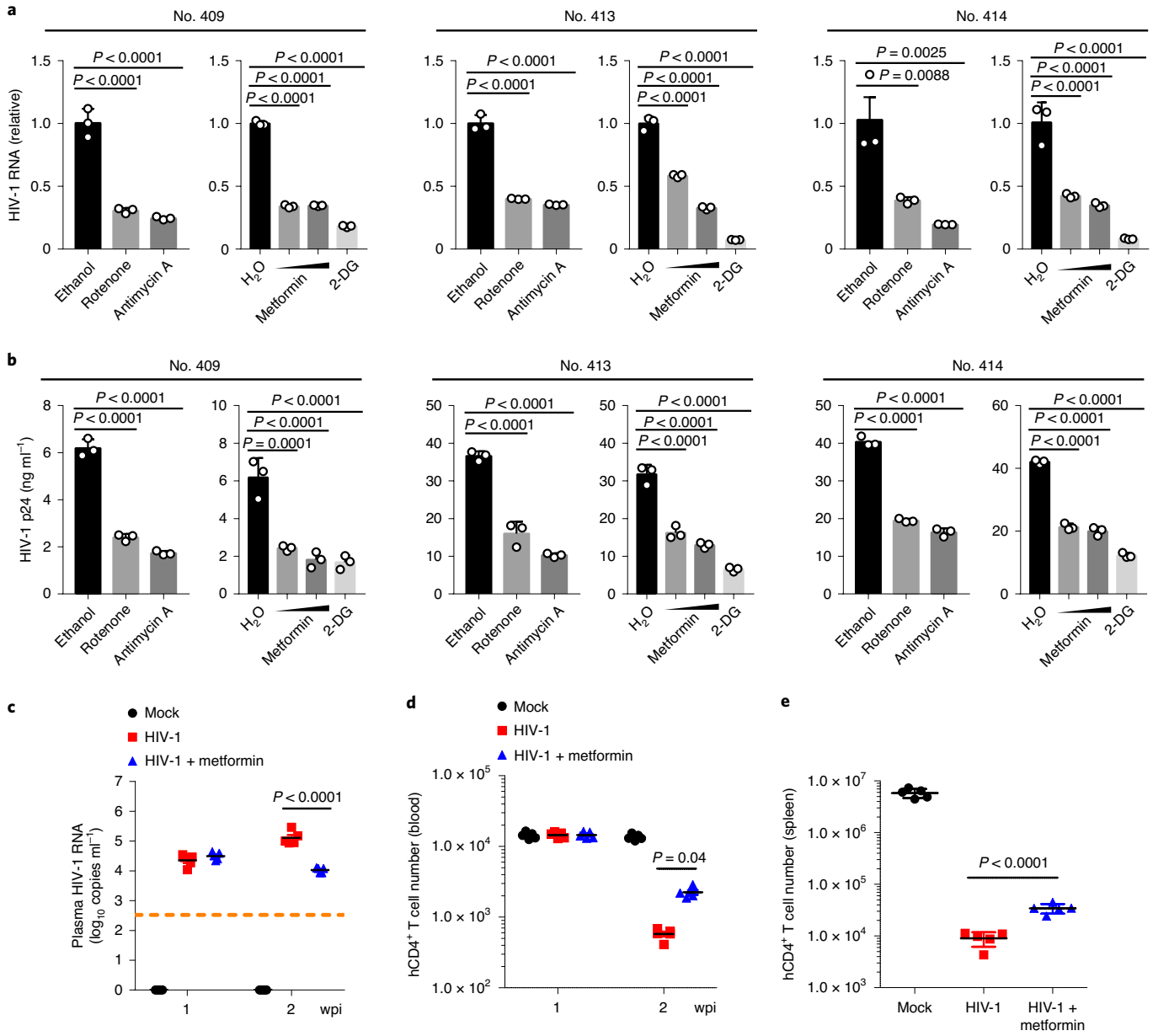

Fig. 2 | Inhibition of OXPHOS reduces HIV-1 replication in human primary CD4⁺ T cells and NRG-hu CD4⁺ mice. a,**b**, Human primary CD4⁺ T cells were infected with three different HIV-1 clinical strains (409, 413 and 414, 10 ng p24) in the presence of rotenone (1 μM), antimycin A (1 μM), metformin (1 mM and 5 mM) or 2-DG (10 mM). Cell-associated HIV-1 RNA (**a**) and cell-released virions (**b**) were assessed by qPCR and p24 ELISA, respectively. Ethanol or sterile water was used as vehicle control ($n = 3$ cell cultures per experiment). **c**, HIV-1 viremia in HIV-1 R3A-infected NRG-hu CD4⁺ mice at 1 and 2 wpi ($n = 5$ mice per group). **d**, Human CD4⁺ T cell counts in peripheral blood of NRG-hu CD4⁺ mice as determined by flow cytometry at 1 and 2 wpi ($n = 5$ mice per group). **e**, Human CD4⁺ T cells in the spleen of NRG-hu CD4⁺ mice as quantified by flow cytometry at 17 d post-infection (dpi) ($n = 5$ mice per group). Representative data of three independent experiments with similar results are presented as mean ± s.e.m. Statistical significance was tested by one-way analysis of variance (ANOVA) with Dunnett's multiple comparisons test (**a**,**b**), two-way ANOVA with Tukey's (**c**) or Šidák's (**d**) multiple comparisons test or unpaired two-tailed Student's *t*-test (**e**).

2 had more than a twofold change, with 210 proteins shared by the two lines as shown by the heat map (Fig. 4a,b and Supplementary Table 4). A distinct protein expression pattern was evident between Jurkat-sh-NLRX1 cells and Jurkat-sh-Ctr cells upon VSV-G-NL4-3-Luc infection, although two infected Jurkat-sh-NLRX1 cell lines showed a similar pattern of enhanced and reduced protein levels compared to Jurkat-sh-Ctr cells (Fig. 4b). When comparing virus-infected cells to uninfected cells, differentially expressed proteins (infection/mock, |fold change| ≥2) in the sh-Ctr group were clustered in the OXPHOS pathway with the most significance (*P* value) and most of the proteins detected in this pathway were upregulated (*z* score) (Fig. 4c). This observation echoed our transcriptomic analysis of the RV217 cohort, showing that OXPHOS positively correlated with HIV-1 set-point viral load. Notably, although proteins in the OXPHOS pathway were predominantly upregulated in Jurkat-sh-Ctr cells upon VSV-G-NL4-3-Luc infection, they were upregulated to a lesser extent in Jurkat-sh-NLRX1 cells (Fig. 4c,d and Supplementary Table 5). The proteome analysis

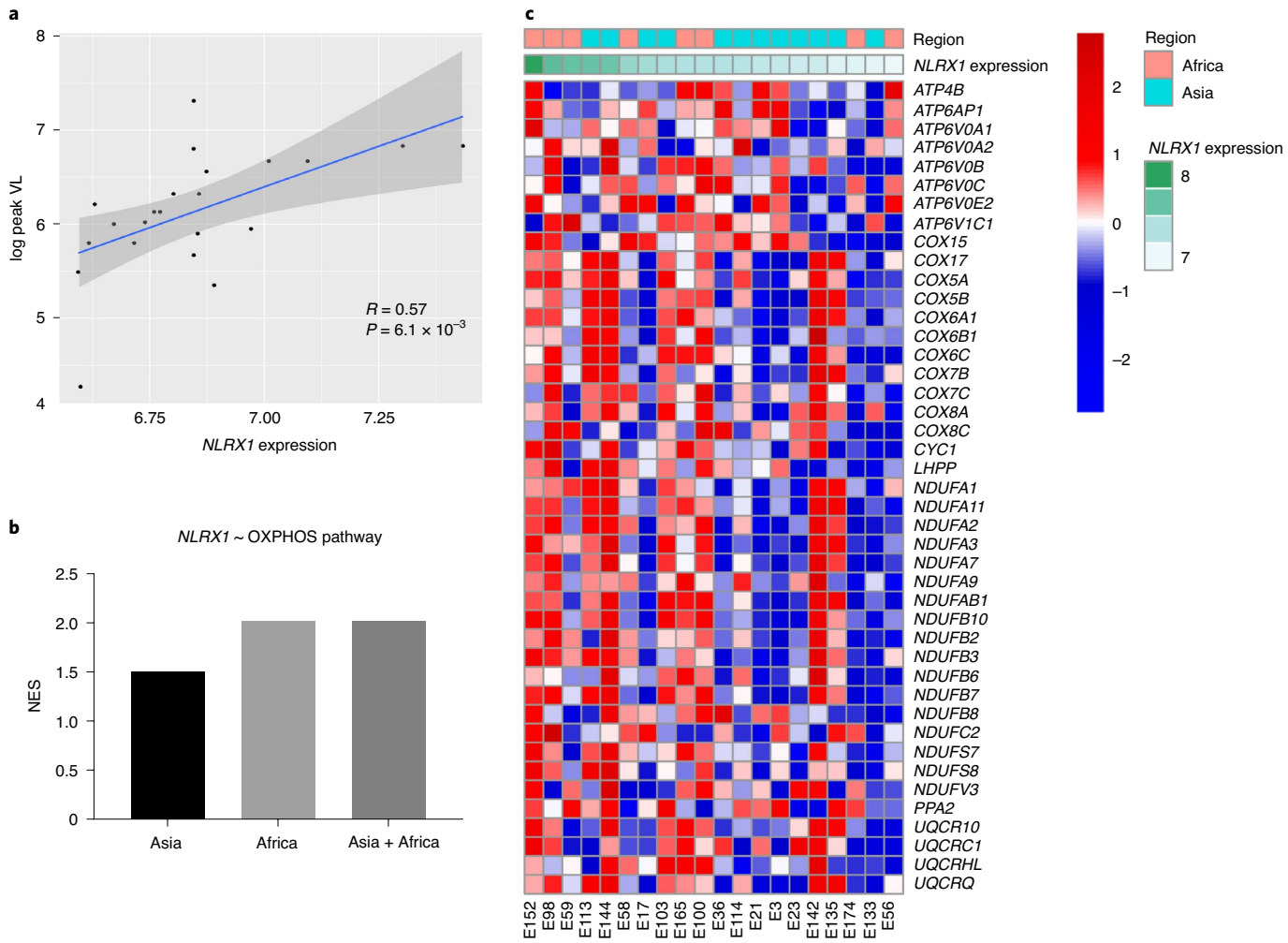

Fig. 3 | *NLRX1* expression positively correlates with HIV-1 viremia and the OXPHOS pathway. a, Scatter-plot highlighting the significant positive correlation between *NLRX1* expression levels (PBMCs, peripheral blood mononuclear cells) and $\log_{10}$ peak VL in the RV217 dataset. A Pearson correlation was used to assess significance. *P* value was not adjusted and was calculated by a one-tailed test. The gray band around the line represents 95% confidence interval. **b**, *NLRX1* expression is positively correlated with OXPHOS pathway gene expression. Linear regression analysis between *NLRX1* and other gene expression was performed using the R package LIMMA, and gene set enrichment analysis (GSEA) was used to assess how the OXPHOS pathway is correlated with the magnitude of *NLRX1* expression in sorted CD4+ T cells from individuals infected with HIV-1 in both Asian and African cohorts. NES reflects the degree to which genes of the OXPHOS pathway are correlated with *NLRX1* expression. Supplementary Table 2 provides statistical results for the enrichment and leading-edge genes of the OXPHOS pathway. **c**, Heat map illustrating leading-edge genes from the OXPHOS pathway that correlate with *NLRX1* expression levels (regression analysis; KEGG, OXPHOS gene set ~*NLRX1* expression levels; GSEA, NES = 2.02, $P < 0.0001$). Rows represent *z* score–normalized genes in the leading-edge of the OXPHOS pathway, and columns represent samples of the RV217 cohort, Africa (red) and Asia (turquoise). The magnitude of *NLRX1* expression (green) is plotted as an annotation at the top of the heat map. Gene expression is represented as a gene-wise standardized expression (*z* score). Red and blue correspond to up- and downregulated genes, respectively.

showed an association of NLRX1 with genes in the OXPHOS pathway; however, it is essential to test whether NLRX1 is a bona fide regulator of OXPHOS during HIV-1 infection by metabolic assays.

NLRX1-depletion did not affect the amount of mitochondrial DNA (Fig. 4e) or OXPHOS in Jurkat cells under the noninfected condition (Fig. 4f); however, there was a substantial increase of OXPHOS in Jurkat-sh-Ctr cells upon VSV-G-NL4-3-Luc infection. This increase was abolished in Jurkat-sh-NLRX1 cells at both basal and maximal respiration and reserved respiratory capacity (Fig. 4f). This indicates that NLRX1 is required for increased OXPHOS upon HIV-1 infection. An increased OXPHOS might be accompanied by increased glycolysis. Indeed, a significant increase of glycolysis and glycolytic capacity was observed upon HIV-1 pseudovirus infection (Fig. 4g), which is in line with the literature[28]. Collectively, these data indicate that NLRX1 is involved in the reprogramming of OXPHOS upon HIV-1 infection of CD4+ T cells.

NLRX1 facilitates HIV-1 replication in human CD4+ T cells. Although NLRX1 suppresses type I interferon (IFN-I) to facilitate HIV-1 replication in myeloid cells[14], whether it regulates HIV-1 replication in its primary target of CD4+ T cells has not been studied. The observed positive correlation between *NLRX1* expression and HIV-1 viremia and increased expression of *NLRX1* upon HIV-1 infection suggested a role of NLRX1 in HIV-1 replication in CD4+ T cells. In line with this hypothesis, HIV-1 replication, reflected by the luciferase activity, decreased three to fivefold in Jurkat-sh-NLRX1 cells compared to Jurkat-sh-Ctr cells over time (Fig. 5a). Consistent with luciferase data, synthesis of HIV-1 Gag

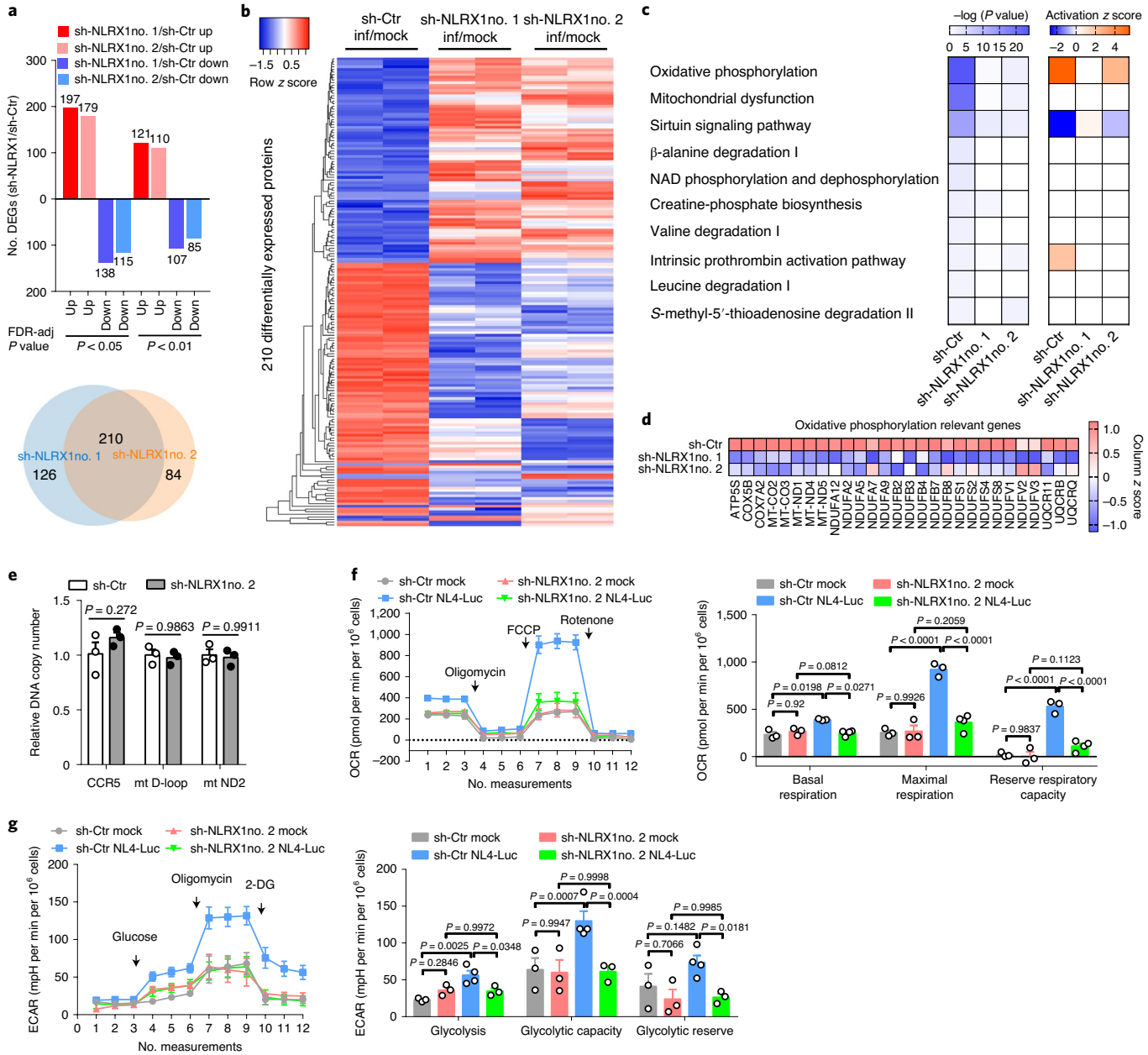

Fig. 4 | NLRX1-dependent upregulation of OXPHOS in HIV-1-infected T cells. a, Bar diagrams represent numbers of upregulated and downregulated proteins in VSV-G-NL4-3-Luc-infected Jurkat-sh-NLRX1 compared to Jurkat-sh-Ctr at indicated levels of false discovery rate (FDR)-adjusted significance (top). Venn diagram shows the number of upregulated and downregulated proteins (sh-NLRX1/sh-Ctr) co-identified using two different NLRX1 shRNA-transduced Jurkat cells (bottom). The 210 co-identified proteins were used to plot the heat map. DEGs, differentially expressed genes. **b**, Heat map comparing the differentially expressed proteins between Jurkat-sh-Ctr and Jurkat-sh-NLRX1 line 1 and Jurkat-sh-NLRX1 line 2 cells infected with VSV-G-NL4-3-Luc. Samples were run in biological duplicates. **c**, Predicted canonical pathways of differentially expressed proteins (infection/mock, fold change ≥2), based on ingenuity pathway analysis (*P* value (left), activation *z* score (right)). **d**, Expression change of proteins involved in the OXPHOS pathway (infection/mock). **e**, The measurement of nuclear and mitochondrial DNA content in Jurkat cells containing sh-Ctr or sh-NLRX1. sh-Ctr was set as 1. For each gene region, $n = 3$ cell cultures per experiment. **f**,**g**, Oxygen consumption rate (OCR) (**f**) and extracellular acidification rate (ECAR) (**g**) in Jurkat-sh-Ctr or Jurkat-sh-NLRX1 cells infected with VSV-G-NL4-3-Luc (NL4-Luc) or left uninfected (mock). Each dot represents one cell culture. Data are the pool (**a**,**b**) or mean (**c**,**d**) of two biological replicates. Data (**e**–**g**) are representative of three independent experiments shown as the mean ± s.e.m. Statistical significance was tested by two-way ANOVA followed by Šidák's (**e**) or Tukey's (**f**,**g**) multiple comparisons test.

protein was also significantly decreased in Jurkat-sh-NLRX1 cells (Fig. 5b). Furthermore, the CCR5/CXCR4 dual-tropic HIV-1 strain R3A also exhibited a dramatic drop of virus replication in Jurkat-sh-NLRX1 cells over time, determined by the quantification of cell-free HIV-1 virions (Fig. 5c) and intracellular staining of HIV-1 capsid antigens p24 (Fig. 5d), respectively. To assess the veracity of these data in primary cells, we decreased *NLRX1* expression in primary human CD4$^+$ T cells with shRNA and found reduced replication of HIV-1 R3A (Fig. 5e). As we have shown, inhibition of OXPHOS could suppress HIV-1 replication. NLRX1

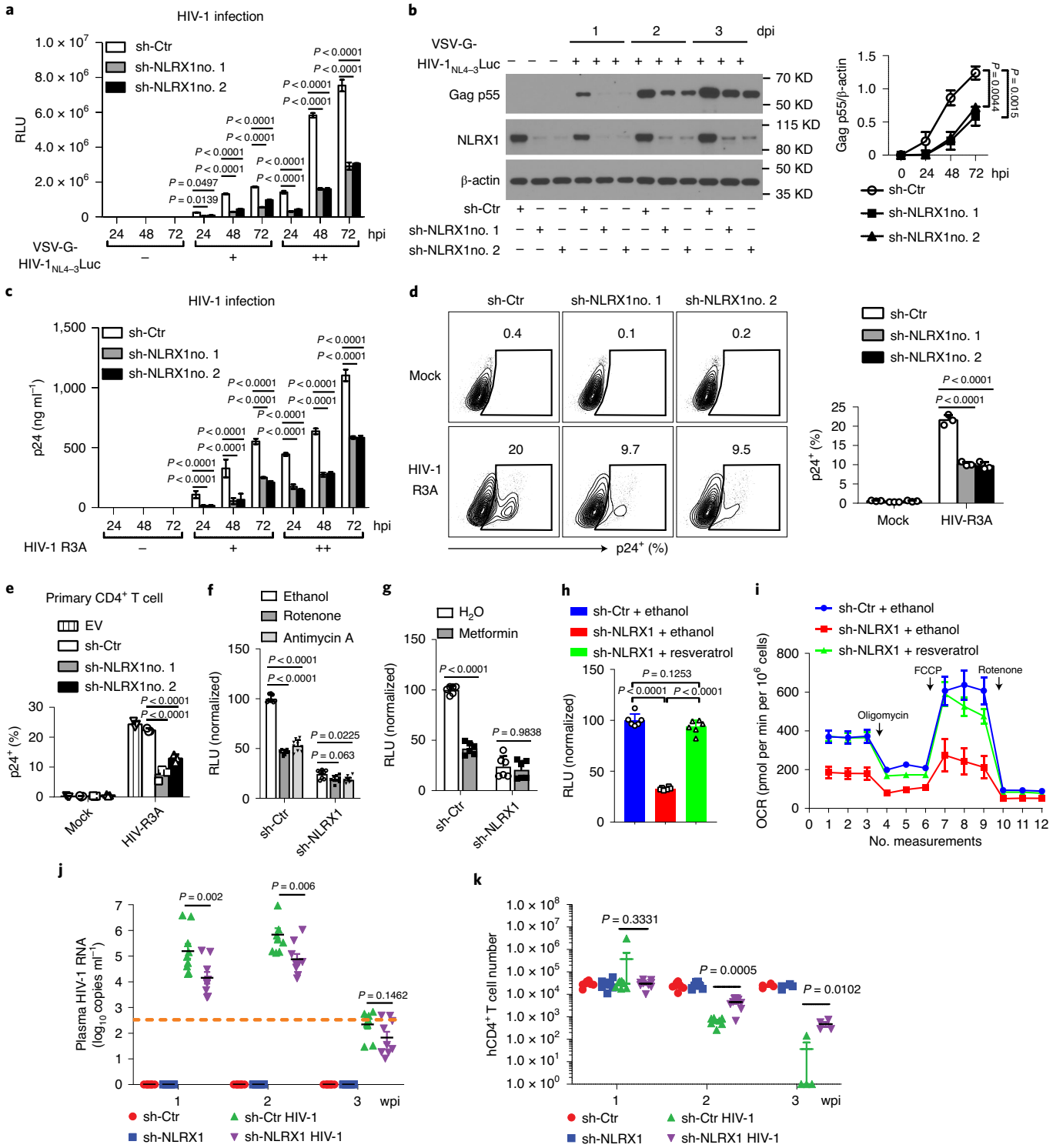

Fig. 5 | NLRX1 is required for HIV-1 replication in human CD4⁺ T cells. a,**b**, Luciferase activities (RLU, relative light units) (**a**) and HIV-1 Gag p55 protein levels (**b**, left). Densitometry analysis of Gag p55 levels (**b**, right). β-actin was the loading control ($n = 3$ cell cultures per experiment). **c**, Extracellular HIV-1 p24 levels ($n = 3$ cell cultures per experiment). **d**, Intracellular HIV-1 p24 levels at 48 hpi ($n = 3$ cell cultures per experiment). **e**, Intracellular HIV-1 p24 levels in *NLRX1*-silenced human primary CD4⁺ T cells at 48 hpi ($n = 3$ cell cultures per experiment). **f**, RLU in 0.2 μM rotenone, 0.2 μM antimycin A or vehicle control ethanol-treated cells at 24 hpi ($n = 9$ cell cultures per experiment). **g**, RLU in 5 mM metformin or vehicle control sterile water–treated cells at 24 hpi ($n = 6$ cell cultures per experiment). **h**, RLU in 5 μM resveratrol or vehicle control ethanol-treated cells at 48 hpi ($n = 6$ cell cultures per experiment). **i**, OCR in 5 μM resveratrol or vehicle control ethanol-treated cells at 24 hpi ($n = 5$ cell cultures per experiment). **j**,**k**, HIV-1 viremia (**j**) and peripheral blood human CD4⁺ T cell count (**k**) in NRG-hu CD4⁺ mice serum ($n = 8$ mice for uninfected and $n = 9$ mice for infected groups). Data (**a**–**i**) are representative of three independent experiments shown as mean ± s.e.m. Data (**j**,**k**) are from pooled mice of two independent experiments. Statistical significance was tested by one-way or two-way ANOVA followed by Tukey's (**a**–**f**,**h**,**j**) or Šidák's (**g**) multiple comparisons test or multiple two-tailed Student's *t*-tests (**k**).

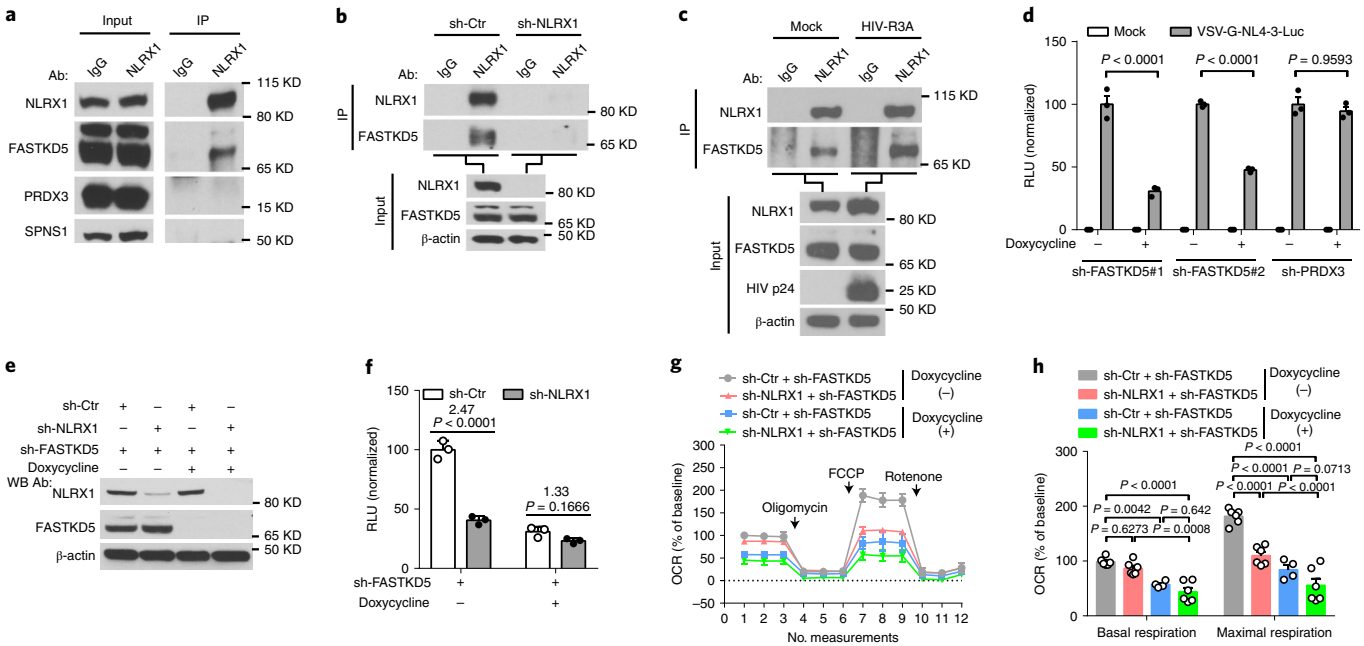

Fig. 6 | NLRX1 associates with FASTKD5 and modulates the OXPHOS pathway and HIV-1 replication in T cells. a, Interactions between NLRX1 and mitochondrial proteins at the endogenous level. Input, cell lysate; IP, immunoprecipitated sample; Ab, antibody; IgG, IP-negative control. **b**, NLRX1 interacted with FASTKD5 at the endogenous level. IgG, IP negative control; β-actin, loading control. **c**, HIV-1 infection enhanced the association of NLRX1 and FASTKD5. HIV-1 R3A-infected Jurkat cells were subjected to IP by NLRX1 antibody or IgG at 72 hpi. β-actin, loading control. **d**, RLU in *FASTKD5*- or *PRDX3*-silenced Jurkat cells at 24 hpi ($n = 3$ cell cultures per experiment). **e**, Jurkat-sh-Ctr and Jurkat-sh-NLRX1 transduced with a lentivirus that contains a Tet-on promoter-controlled shRNA for *FASTKD5* were treated with doxycycline for 72 h or left untreated. Immunoblot shows silencing of *FASTKD5* and *NLRX1*. WB, western blot. β-actin, loading control. **f**, Cells were treated as described in **e**, followed by infection with VSV-G-NL4-3-Luc. RLU was measured at 24 hpi ($n = 3$ cell cultures per experiment). **g**, Silencing of *FASTKD5* in Jurkat-sh-Ctr and Jurkat-sh-NLRX1 was induced by doxycycline for 72 h, followed by infection of VSV-G-NL4-3-Luc. OCR was determined at 24 hpi ($n = 6$ cell cultures per experiment). **h**, Basal respiration and maximal respiration. Each dot represents one cell culture. Data are representative of three independent experiments and **d**,**f**–**h** are shown as mean ± s.e.m. Statistical significance was tested by two-way ANOVA followed by Tukey's (**d**,**h**) or Šidák's (**f**) multiple comparisons test.

was required for upregulation of OXPHOS upon HIV-1 infection in CD4⁺ T cells. Therefore, a possible model is that NLRX1 would promote HIV-1 replication in CD4⁺ T cells via OXPHOS. In fact, OXPHOS inhibitors, rotenone, antimycin A and metformin, which significantly suppressed HIV-1 replication in Jurkat-sh-Ctr cells, had less or no effect on HIV-1 replication in Jurkat-sh-NLRX1 cells, indicating that the effect of OXPHOS on HIV-1 replication is NLRX1-dependent (Fig. 5f,g). Interestingly, *NLRX1* expression was significantly increased in metformin-treated primary CD4⁺ T cells (Extended Data Fig. 4), which may reflect compensatory feedback for the reduced OXPHOS by metformin. More notably, resveratrol, which can upregulate the expression of electron transport chain constituents[29,30], restored both HIV-1 replication (Fig. 5h) and OXPHOS (Fig. 5i) in Jurkat-sh-NLRX1 cells to a similar level as in control cells. Collectively, these results suggest that NLRX1 is a host factor that promotes HIV-1 replication in CD4⁺ T cells via the OXPHOS pathway.

Diminishing NLRX1 reduces HIV-1 replication in humanized mice reconstituted with human CD4⁺ T cells. To investigate the function of NLRX1 in HIV-1 replication in vivo, NRG mice were reconstituted with human CD4⁺ T cells containing sh-NLRX1 or sh-Ctr, infected with HIV-1 and monitored for viremia and human CD4⁺ T cell count weekly. Consistent with results from in vitro CD4⁺ T cell cultures, NRG-hu CD4⁺ mice containing sh-NLRX1 had a one-order-of-magnitude drop in viral load in peripheral blood over time when compared to those with sh-Ctr (Fig. 5j). Reducing *NLRX1* expression did not affect human CD4⁺ T cell reconstitution, demonstrated by similar CD4⁺ T cell counts in peripheral blood of NRG-hu CD4⁺ mice bearing sh-Ctr or sh-NLRX1 before HIV-1 infection (Fig. 5k). Human CD4⁺ T cells were depleted by HIV-1, starting from 2 wpi in the NRG-hu CD4⁺ model. In line with viral load data, diminishing NLRX1 resulted in protection of human CD4⁺ T cells from depletion, demonstrated by nearly a log higher CD4⁺ T cell count in peripheral blood of NRG-hu CD4⁺ mice bearing sh-NLRX1 assayed at 2 and 3 wpi (Fig. 5k and Extended Data Fig. 5a). In addition to peripheral blood, silence of NLRX1 also significantly protected human CD4⁺ T cells from depletion by HIV-1 in the NRG-hu CD4⁺ mouse spleen, reflected by an attenuated reduction of spleen size and splenocyte counts (Extended Data Fig. 5b,c). Together, these data indicate that diminishing NLRX1 partially protected CD4⁺ T cells from HIV-1-mediated depletion by suppressing viral replication in vivo.

Endogenous NLRX1 interacts with endogenous FASTKD5 to promote HIV-1 replication. To decipher the mechanism underlying NLRX1-regulated cellular metabolism and HIV-1 replication in CD4⁺ T cells, we first examined the previously reported functions of NLRX1. In addition to regulating IFN-I responses, NLRX1 has been reported to promote autophagy and endoplasmic reticulum (ER) stress[31,32]. As IFN-I produced by CD4⁺ T cells is too low to limit HIV-1 replication at the first round[33], the role of NLRX1 in CD4⁺ T cells is unlikely to be attributed to IFN-I. Indeed, blockage of IFN-I downstream signaling with the Janus kinase inhibitor, ruxolitinib, did not affect HIV-1 replication in either Jurkat-sh-Ctr or Jurkat-sh-NLRX1 cells (Extended Data Fig. 6a), although it did diminish the

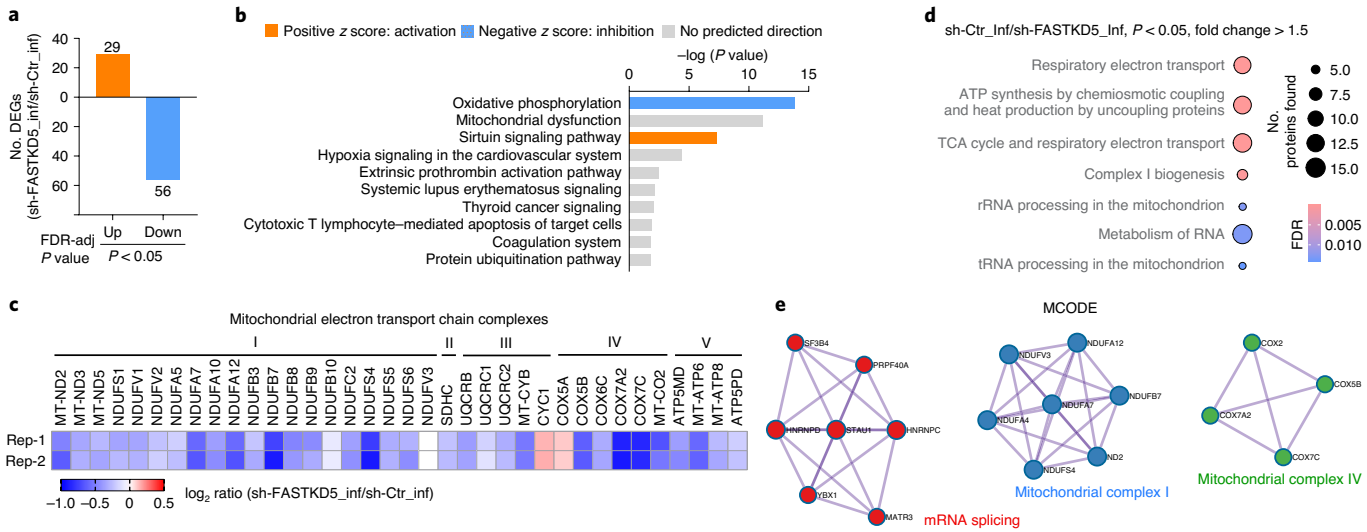

Fig. 7 | FASTKD5 upregulates electron transport chain components upon HIV-1 infection. a, Characterization of FASTKD5-regulated protein expression by tandem mass tag (TMT)-based quantitative mass spectrometry. Bar diagrams represent numbers of upregulated and downregulated proteins in VSV-G-NL4-3-Luc-infected Jurkat cells induced by doxycycline to express shRNA against *FASTKD5* (sh-FASTKD5) compared to un-induced Jurkat cells (sh-Ctr) at indicated levels of FDR-adjusted significance. The mean value of two biological replicates was used to calculate the fold change (FC; sh-FASTKD5/sh-Ctr). Proteins with |FC| > 1.5 and FDR < 0.05 were identified as differentially expressed proteins. **b**, Predicted canonical pathways of differentially expressed proteins based on ingenuity pathway analysis. Top ten enriched pathways based on *P* value were plotted. Positive *z* score indicating activation was presented in orange and negative *z* score indicating inhibition was presented in blue. **c**, Heat map presenting changes in expression of proteins in mitochondrial electron transport chain complexes (sh-FASTKD5/sh-Ctr, VSV-G-NL4-3-Luc infection). Samples were run in biological duplicates. *P* value < 0.05 was used as the filter. **d**, ReactomeFI network analysis of proteins downregulated in **a**. Circle size represents number of proteins found in the pathway and color shows FDR for enrichment. Pathways with FDR < 0.05 were plotted. **e**, MCODE analysis of proteins downregulated in **a** was performed by Metascape.

phosphorylation of STAT1, indicating the efficacy of the inhibitor (Extended Data Fig. 6b). An autophagy inhibitor 3-methyladenine (3-MA) significantly but equally suppressed VSV-G-NL4-3-Luc replication in Jurkat-sh-Ctr or Jurkat-sh-NLRX1 cells, suggesting that NLRX1-regulated HIV-1 replication is independent of the autophagy pathway (Extended Data Fig. 6c). Pharmacological inhibition of ER stress did not alter VSV-G-NL4-3-Luc replication in either Jurkat-sh-Ctr or Jurkat-sh-NLRX1 cells (Extended Data Fig. 6d), suggesting that this pathway is also not involved. These experiments excluded previously known functions of NLRX1 as the molecular basis of its enhancement of HIV-1 replication in $CD4^+$ T cells and justified a focus on the link of NLRX1-regulated metabolic changes with HIV-1 replication.

To explore this unknown mechanism, we searched NLRX1 interaction proteins based on a published database describing interaction networks of innate immune proteins by the co-immunoprecipitation and mass spectrometry approach[34]. NLRX1 resides in the mitochondria and potentially regulates OXPHOS by interacting with its mitochondrial partners. Mitochondrial proteins FASTKD5, PRDX3 and SPNS1 were screened as NLRX1 interaction partners previously using overexpressed NLRX1 as the bait for immunoprecipitation followed by mass spectrometry (Extended Data Fig. 7a)[34]. We assessed the physiological relevance of these interactions by examining interactions between the endogenous proteins in T cells. A strong specific association was detected between endogenous NLRX1 and FASTKD5 (Fig. 6a,b), whereas NLRX1–PRDX3 and NLRX1–SPNS1 interactions were not detected (Fig. 6a). Further, HIV-1 infection enhanced the interaction between NLRX1 and FASTKD5, although it did not alter FASTKD5 expression at both the transcript and protein level (Fig. 6c and Extended Data Fig. 7b,c).

We next tested the hypothesis that NLRX1 and FASTKD5 work together to regulate OXPHOS and HIV-1 replication in T cells. To test the role of FASTKD5, we silenced *FASTKD5* expression in Jurkat cells by doxycycline-inducible shRNA, and we also silenced a negative control PRDX3 that did not endogenously interact with NLRX1 in our validation experiment (Extended Data Fig. 7d,e). This was followed by VSV-G-NL4-3-Luc infection. Silencing *FASTKD5* resulted in significant suppression of viral replication at 24 h post-infection (hpi) (Fig. 6d). Silencing *PRDX3* showed no significant effect on viral replication (Fig. 6d). The latter excluded the unintended effect from doxycycline treatment and provided a specificity control. Silencing *FASTKD5* in Jurkat cells that also silenced NLRX1 with sh-NLRX1 did not further reduce VSV-G-NL4-3-Luc replication, suggesting that these two proteins are in the same pathway and thus exhibited redundant activity (Fig. 6e,f). Similar to the earlier study showing that the silencing of *NLRX1* dampened HIV-1-induced upregulation of OXPHOS, silencing *FASTKD5* also reduced OXPHOS (Fig. 6g,h). Again, silencing both *NLRX1* and *FASTKD5* provided no significant additive effect over the silencing of each individual gene in their impact on OXPHOS, reinforcing the concept that these two are in the same pathway (Fig. 6g,h). Taken together, these results identified a new NLRX1- and FASTKD5-dependent pathway that regulates HIV-1 replication and the OXPHOS state of HIV-1-infected T cells.

Silencing *FASTKD5* generally reduces the expression of mitochondrial electron transport chain components. To further explore the molecular mechanism underlying FASTKD5-regulated OXPHOS in the context of HIV-1 infection, we profiled the proteome of HIV-1 pseudovirus-infected *FASTKD5*-silenced Jurkat cells (sh-FASTKD5_inf) and its control cells (sh-Ctr_inf) by quantitative mass spectrometry. Compared to control cells, the differentially expressed proteins (|fold change| ≥1.5, $P < 0.05$) showed more downregulation than upregulation in *FASTKD5*-silenced

cells (Fig. 7a and Supplementary Table 6). When analyzing by ingenuity pathway analysis, these differentially expressed proteins (sh-FASTKD5_inf/sh-Ctr_inf) were most enriched in the OXPHOS pathway with a negative *z* score, suggesting downregulation of OXPHOS in *FASTKD5*-silenced Jurkat cells (Fig. 7b). In line with this, we observed a general decrease of electron transport chain components, which spanned mitochondrial complex-I to V (Fig. 7c). To pinpoint how FASTKD5 regulates protein levels in the OXPHOS pathway, we performed ReactomeFI network analysis of downregulated proteins in *FASTKD5*-silenced cells and found that, in addition to clustered pathways involved in mitochondrial respiration and metabolism of RNA and mitochondrial ribosomal RNA and transfer RNA processing were enriched (Fig. 7d). By performing molecular complex detection (MCODE), we found that mitochondrial complex-I and IV and notably, a molecular complex for mRNA splicing were among the downregulated proteins (Fig. 7e). The proteomic analysis agrees with previous reports that FASTKD5 binds to mitochondrial rRNA and mRNA, which is critical for mitochondrial mRNA maturation and subsequent mitochondrial protein translation and electron transport chain complex assembly[35,36]. Thus, combined with the proteomic analysis of *NLRX1*-silenced T cells in the context of HIV-1 infection (Fig. 4d), we found both NLRX1 and FASTKD5 positively regulate expression of genes in the OXPHOS pathway. These data reinforced the concept that NLRX1 and FASTKD5 cooperatively promote OXPHOS in HIV-1-infected T cells.

Discussion

Immunometabolism is altered in individuals with HIV-1. Although metabolic reprogramming is associated with persistent HIV-1 spontaneous control by $CD8^+$ T cells[37], the metabolic signatures of $CD4^+$ T cells accountable for HIV-1 disease progression are unclear[3]. In this study, we took advantage of the RV217 Early Capture HIV Cohort Study in which the patient's HIV status and progression were characterized through the acute stages of HIV infection[20]. We analyzed the transcriptome of $CD4^+$ T cells and found that expression of genes in the OXPHOS pathway positively correlates with HIV-1 set-point viral load. As a higher level of HIV-1 set-point viral load is usually associated with a faster progression to AIDS[21], it is reasonable to recognize OXPHOS as a metabolic signature in the acute infection phase for predicting AIDS progression.

It was previously shown that HIV-1 preferentially infects $CD4^+$ T cells harboring a higher glycolytic and respiratory activity, but whether and how HIV-1 infection directly alters glycolysis and OXPHOS pathways are unclear[6]. This study used single-round replication HIV-1 pseudovirus VSV-G-NL4-3-Luc and found that both OXPHOS and glycolysis are upregulated upon virus infection. Meanwhile, by using quantitative mass spectrometry, we found an enrichment of genes in the OXPHOS pathway with the most significance among all the canonical pathways analyzed by ingenuity pathways analysis.

A notable finding in our study is that mitochondria-localized innate immune protein NLRX1 and FASTKD5 mediate upregulation of OXPHOS in HIV-1-infected $CD4^+$ T cells. Mechanistically, NLRX1 associates with FASTKD5, a mitochondrial protein critical for mitochondrial protein translation and respiratory complexes assembly by binding with and processing mitochondrial RNA[35,36]. This study shows the NLRX1–FASTKD5 interaction at the endogenous expression level in $CD4^+$ T cells. This association is increased in HIV-1-infected cells over uninfected cells. Silencing either *NLRX1* or *FASTKD5* in $CD4^+$ T cells dampened expression of genes in the OXPHOS pathway and mitochondrial respiration. It is notable that, based on our proteome data, the restricted expression of OXPHOS proteins by silencing *NLRX1* or *FASTKD5* was not limited to mitochondrial-encoded electron transport complex components but extended to nuclear-encoded components. A possible explanation is that reduced mitochondrial proteins cause mitochondrial respiration dysfunction, which dampens cellular metabolism and, thereafter, general gene expression.

In line with NLRX1 and FASTKD5-orchestrated upregulation of OXPHOS in HIV-1-infected $CD4^+$ T cells, both genes are required for HIV-1 replication in $CD4^+$ T cells. Currently, it is challenging to target NLRX1 and FASTKD5 for treating HIV-1 infection due to the lack of commercialized inhibitors; thus, we used regulators of OXPHOS to modulate HIV-1 replication. We showed that the FDA-approved antidiabetic agent metformin, which is shown to suppress OXPHOS by targeting mitochondrial complex-I, reduced HIV-1 replication in primary $CD4^+$ T cells in vitro and in mice reconstituted with human $CD4^+$ T cells in vivo. Notably, clinical data showed that individuals with both HIV-1 and type 2 diabetes mellitus comorbidity exhibited an average 1.33-fold lower HIV-1 viral load than patients with HIV without diabetes among the early cART-treated cohort (6 months)[38]. In line with viral load data, patients with both HIV and type 2 diabetes mellitus had a higher $CD4^+$ T cell baseline and faster recovery of $CD4^+$ T cell number after cART, which was correlated with metformin use[38,39]. These clinical observations strengthen the supplementation of early-stage cART with drugs such as metformin to further restrict HIV-1 replication in patients. The toxic side effects of cART usually leads to treatment interruption, which results in a rebound of HIV-1 viremia and a decline in $CD4^+$ T cells[40]. Administration of metformin during cART interruption may delay the rebound of HIV-1 viremia and offer a more extended period before the next round of cART. It is noted that the safety of administration of metformin for patients with HIV, especially combined with cART, remains to be explored. A clinical trial (NCT02659306) registered to treat nondiabetic patients with HIV-1 with metformin combined with anti-HIV drugs will shed light on the safety and effectiveness of metformin in nondiabetic patients with HIV [41].

In conclusion, we discovered a critical role of OXPHOS in HIV-1 replication in $CD4^+$ T cells and a new NLRX1 and FASTKD5-dependent mechanism underlying immunometabolism regulation by HIV-1 in $CD4^+$ T cells. These findings build the premise to repurpose drugs that target OXPHOS for the treatment of HIV-1 infection.

Online content

Any methods, additional references, Nature Research reporting summaries, source data, extended data, supplementary information, acknowledgements, peer review information; details of author contributions and competing interests; and statements of data and code availability are available at https://doi.org/10.1038/s41590-021-00898-1.

Received: 21 March 2020; Accepted: 8 February 2021;
Published online: 25 March 2021

References

1. Gaardbo, J. C., Hartling, H. J., Gerstoft, J. & Nielsen, S. D. Incomplete immune recovery in HIV infection: mechanisms, relevance for clinical care, and possible solutions. *Clin. Dev. Immunol.* **2012**, 670957 (2012).
2. Palmer, C. S. et al. Increased glucose metabolic activity is associated with $CD4^+$ T-cell activation and depletion during chronic HIV infection. *AIDS* **28**, 297–309 (2014).
3. Palmer, C. S., Palchaudhuri, R., Albargy, H., Abdel-Mohsen, M. & Crowe, S. M. Exploiting immune cell metabolic machinery for functional HIV cure and the prevention of inflammaging. *F1000Res* **7**, 125 (2018).
4. Dagenais-Lussier, X. et al. Current topics in HIV-1 pathogenesis: the emergence of deregulated immuno-metabolism in HIV-infected subjects. *Cytokine Growth Factor Rev.* **26**, 603–613 (2015).
5. Gerriets, V. A. & Rathmell, J. C. Metabolic pathways in T cell fate and function. *Trends Immunol.* **33**, 168–173 (2012).
6. Valle-Casuso, J. C. et al. Cellular metabolism is a major determinant of HIV-1 reservoir seeding in $CD4^+$ T cells and offers an opportunity to tackle infection. *Cell Metab.* **29**, 611–626 (2019).

7. Palmer, C. S. et al. Glucose transporter 1–expressing proinflammatory monocytes are elevated in combination antiretroviral therapy–treated and untreated HIV$^+$ subjects. *J. Immunol.* **193**, 5595–5603 (2014).
8. Korencak, M. et al. Effect of HIV infection and antiretroviral therapy on immune cellular functions. *JCI Insight* **4**, e126675 (2019).
9. Xia, X. et al. NLRX1 negatively regulates TLR-induced NF-κB signaling by targeting TRAF6 and IKK. *Immunity* **34**, 843–853 (2011).
10. Moore, C. B. et al. NLRX1 is a regulator of mitochondrial antiviral immunity. *Nature* **451**, 573–577 (2008).
11. Allen, I. C. et al. NLRX1 protein attenuates inflammatory responses to infection by interfering with the RIG-I-MAVS and TRAF6-NF-κB signaling pathways. *Immunity* **34**, 854–865 (2011).
12. Koblansky, A. A. et al. The innate immune receptor NLRX1 functions as a tumor suppressor by reducing colon tumorigenesis and key tumor-promoting signals. *Cell Rep.* **14**, 2562–2575 (2016).
13. Stokman, G. et al. NLRX1 dampens oxidative stress and apoptosis in tissue injury via control of mitochondrial activity. *J. Exp. Med.* **214**, 2405–2420 (2017).
14. Guo, H. et al. NLRX1 sequesters STING to negatively regulate the interferon response, thereby facilitating the replication of HIV-1 and DNA viruses. *Cell Host Microbe* **19**, 515–528 (2016).
15. Barouch, D. H. et al. Rapid inflammasome activation following mucosal SIV infection of rhesus monkeys. *Cell* **165**, 656–667 (2016).
16. Chan, E. Y. et al. Dynamic host energetics and cytoskeletal proteomes in human immunodeficiency virus type 1-infected human primary CD4 cells: analysis by multiplexed label-free mass spectrometry. *J. Virol.* **83**, 9283–9295 (2009).
17. Ringrose, J. H., Jeeninga, R. E., Berkhout, B. & Speijer, D. Proteomic studies reveal coordinated changes in T-cell expression patterns upon infection with human immunodeficiency virus type 1. *J. Virol.* **82**, 4320–4330 (2008).
18. Stanley, T. L. & Grinspoon, S. K. Body composition and metabolic changes in HIV-infected patients. *J. Infect. Dis.* **205**, S383–S390 (2012).
19. Valle-Casuso, J. C. et al. Cellular metabolism is a major determinant of HIV-1 reservoir seeding in CD4$^+$ T cells and offers an opportunity to tackle infection. *Cell Metab.* https://doi.org/10.1016/j.cmet.2018.11.015 (2019).
20. Robb, M. L. et al. Prospective study of acute HIV-1 infection in adults in East Africa and Thailand. *N. Engl. J. Med.* **374**, 2120–2130 (2016).
21. Mellors, J. W. et al. Prognosis in HIV-1 infection predicted by the quantity of virus in plasma. *Science* **272**, 1167–1170 (1996).
22. Kelley, C. F., Barbour, J. D. & Hecht, F. M. The relation between symptoms, viral load, and viral load set point in primary HIV infection. *J. Acquir. Immune Defic. Syndr.* **45**, 445–448 (2007).
23. Wheaton, W. W. et al. Metformin inhibits mitochondrial complex I of cancer cells to reduce tumorigenesis. *Elife* **3**, e02242 (2014).
24. Ye, C. et al. Glycosylphosphatidylinositol-anchored anti-HIV scFv efficiently protects CD4 T cells from HIV-1 infection and deletion in hu-PBL mice. *J. Virol.* https://doi.org/10.1128/JVI.01389-16 (2017).
25. Martin-Montalvo, A. et al. Metformin improves healthspan and lifespan in mice. *Nat. Commun.* **4**, 2192 (2013).
26. McCune, J. M. The dynamics of CD4$^+$ T-cell depletion in HIV disease. *Nature* **410**, 974–979 (2001).
27. Pernicova, I. & Korbonits, M. Metformin—mode of action and clinical implications for diabetes and cancer. *Nat. Rev. Endocrinol.* **10**, 143–156 (2014).
28. Hegedus, A., Kavanagh Williamson, M. & Huthoff, H. HIV-1 pathogenicity and virion production are dependent on the metabolic phenotype of activated CD4$^+$ T cells. *Retrovirology* **11**, 98 (2014).
29. Lagouge, M. et al. Resveratrol improves mitochondrial function and protects against metabolic disease by activating SIRT1 and PGC-1α. *Cell* **127**, 1109–1122 (2006).
30. Csiszar, A. et al. Resveratrol induces mitochondrial biogenesis in endothelial cells. *Am. J. Physiol. Heart Circ. Physiol.* **297**, H13–H20 (2009).
31. Lei, Y. et al. The mitochondrial proteins NLRX1 and TUFM form a complex that regulates type I interferon and autophagy. *Immunity* **36**, 933–946 (2012).
32. Lei, Y. et al. EGFR-targeted mAb therapy modulates autophagy in head and neck squamous cell carcinoma through NLRX1–TUFM protein complex. *Oncogene* **35**, 4698–4707 (2016).
33. Vermeire, J. et al. HIV triggers a cGAS-dependent, Vpu- and Vpr-regulated type I interferon response in CD4$^+$ T cells. *Cell Rep.* **17**, 413–424 (2016).
34. Li, S., Wang, L., Berman, M., Kong, Y. Y. & Dorf, M. E. Mapping a dynamic innate immunity protein interaction network regulating type I interferon production. *Immunity* **35**, 426–440 (2011).
35. Jourdain, A. A. et al. A mitochondria-specific isoform of FASTK is present in mitochondrial RNA granules and regulates gene expression and function. *Cell Rep.* **10**, 1110–1121 (2015).
36. Antonicka, H. & Shoubridge, E. A. Mitochondrial RNA granules are centers for posttranscriptional RNA processing and ribosome biogenesis. *Cell Rep.* **10**, 920–932 (2015).
37. Tarancon-Diez, L. et al. Immunometabolism is a key factor for the persistent spontaneous elite control of HIV-1 infection. *EBioMedicine* **42**, 86–96 (2019).
38. Zuniga, J. A., Easley, K. A., Shenvi, N., Nguyen, M. L. & Holstad, M. The impact of diabetes on CD4 recovery in persons with HIV in an urban clinic in the United States. *Int J. STD AIDS* **29**, 63–71 (2018).
39. Moyo, D. et al. Cohort study of diabetes in HIV-infected adult patients: evaluating the effect of diabetes mellitus on immune reconstitution. *Diabetes Res. Clin. Pr.* **103**, e34–e36 (2014).
40. Carr, A. Toxicity of antiretroviral therapy and implications for drug development. *Nat. Rev. Drug Discov.* **2**, 624–634 (2003).
41. Routy, J. P. et al. Effect of metformin on the size of the HIV reservoir in non-diabetic ART-treated individuals: single-arm non-randomised Lilac pilot study protocol. *BMJ Open* **9**, e028444 (2019).

Methods

Ethics statement. All experiments using animals and human blood were conducted according to guidelines for the housing and care of laboratory animals[42] and in accordance with protocols approved by the Institutional Animal Care and Use Committee and Institutional Review Boards at the University of North Carolina at Chapel Hill (UNC-CH). Human blood was purchased from the Gulf Coast Regional Center. The protocol for RV217 study was approved by the local ethics review boards and the Walter Reed Army Institute of Research. Written informed consent was obtained from all participants.

Cell culture. Jurkat cells (TIB-152, ATCC) and derived lines were maintained in RPMI1640 medium (Gibco) containing 10% fetal bovine serum (FBS), 1% penicillin and 100 μg ml^{-1} streptomycin (hereafter referred to as complete RPMI medium). HEK293T cells (CRL-3216, ATCC) were maintained in DMEM (Gibco) containing 10% FBS, 1% penicillin and 100 μg ml^{-1} streptomycin. All cell lines were tested as mycoplasma-free. Human primary CD4$^+$ T cells isolated from human PBMCs using Dynabeads human CD4$^+$ T cell kit (11352D, Invitrogen) were stimulated and expanded with anti-CD3/anti-CD28-coated magnetic beads (11131D, Gibco) at a bead-to-cell ratio of 1:1 and maintained in a complete RPMI medium supplemented with 200 IU ml^{-1} interleukin-2 (National Institutes of Health (NIH) AIDS Reagent Program).

Virus propagation and infection. Single-round virus vectors pNL4-3.Luc.E-R- were obtained from the NIH AIDS Reagent Program and pNL4-3.EGFP.E- was shared by S. K. Chanda at Sanford Burnham Prebys Medical Discovery Institute. VSV-G-pseudotyped HIV was produced as described previously[43]. Viruses were concentrated (30-fold) using the Lenti concentrator (TR30026, OriGene). Viral titer was determined by intracellularly staining with HIV-1 p24 antibody (KC57-FITC, Beckman Coulter) at 3 dpi. HIV-1 R3A was produced by transfecting proviral plasmid into HEK293T cells as described previously[44]. Virions were quantified by the HIV-1 p24 Antigen Capture Assay kit (NIH AIDS Reagent Program). HIV-1 clinical isolates recovered from human resting CD4$^+$ cells from HIV-1-infected donors were provided by D. Margolis (UNC-CH). Jurkat and human primary CD4$^+$ T cells were infected with VSV-G-pseudotyped HIV-1, HIV-1 R3A or HIV-1 clinical isolates in the presence of 8 μg ml^{-1} polybrene (TR-1003-G, Sigma-Aldrich) at the multiplicity of infection (MOI) indicated in figure legends or below. For drug treatment, 2.5 mM 3-MA (tlrl-3ma, Invivogen), 200 μM tauroursodeoxycholate (T0266, Sigma-Aldrich), 0.2 or 1 μM rotenone (R8875, Sigma-Aldrich), 0.2 or 1 μM antimycin A (R8674, Sigma-Aldrich), 1 or 5 mM metformin (PHR1084, Sigma-Aldrich), 5 or 10 mM 2-DG (D8375, Sigma-Aldrich) or 5 μM resveratrol (R5010, Sigma-Aldrich) was used to treat cells 1 h before and during virus infection.

Real-time PCR and oligonucleotides. Total cellular RNA was extracted using TRIzol reagent at indicated time points in figure legends, followed by reverse transcription by iScript cDNA Synthesis kit (1708891, Bio-Rad). *NLRX1*, *FASTKD5*, *GAPDH* or *ACTB* TaqMan gene expression assay (Hs00226360_m1, Hs01855817_s1, Hs02758991_g1 or Hs99999903_m1, Applied Biosystems) was used to quantify gene expression by real-time PCR. HIV-1 replication was quantified by real-time PCR using the probe (FAM-5′-AAAATTCGGTTAAGGCCAGGGGGAAAGAA-3′-TAMRA, Applied Biosystems) and primers (5′-GGTGCGAGAGCGTCAGTATTAAG-3′, 5′-AGCTCCCTGCTTGCCCATA-3′, Integrated DNA Technologies) targeting the HIV-1 Gag region. Gene expressions were normalized to *ACTB* or *GAPDH* mRNA levels. Cellular DNA was extracted from 2×10^5 cells using a DNeasy Blood and Tissue kit (QIAGEN). Mitochondrial DNA (within D-loop or *MT-ND2*) and nuclear DNA (within nuclear gene *CCR5*) content was measured by real-time PCR using SYBR Green (4309155, Applied Biosystems) and normalized by the nuclear DNA (within TBP nuclear regions on chromosome 6). Primers used were *CCR5*: 5′-CCAGAAGAGCTGAGACATCCG-3′, 5′-GCCAAGC AGCTGAGAGGTTACT-3′; D-loop: 5′-GATTTGGGTACCACCCAAGTATTG-3′, 5′-GTACAATATTCATGGTGGCTGGCA-3′; *MT-ND2*: 5′-AGCACCACGACCC TACTACT-3′, 5′-TGGTGGGGATGATGAGGCTA-3′; and *TBP*: 5′-TTCAC TTCCCCTTGGCCACAACAT-3′, 5′-TGTTCCATGCAGGGGAAAACAAGC-3′. Analyses for relative gene expression, mitochondrial DNA content and HIV-1 replication were performed using the $2^{-\Delta\Delta CT}$ approach[45].

Lentiviruses preparation and cell transduction. TRC lentiviral pLKO.1 empty vector and pLKO.1 containing *NLRX1* targeting shRNAs (TRCN0000128446, sh-NLRX1 line 1: 5′- GTCTGGAATCTCCAAGTTAAA -3′, TRCN0000130325, sh-NLRX1 line 2: 5′- GAGTCTGGAATCTCCAAGTTA -3′) were obtained from TRC-Hs1.0 (human) library provided by the Lenti-shRNA Core Facility at UNC-CH. TRC lentiviral nontargeting shRNA (sh-Ctr) was purchased from Horizon Discovery (catalog no. RHS6848). SMARTvector inducible lentiviral shRNA targeting *FASTKD5* (sh-FASTKD5 line 1: V3SH11252-226616423 and sh-FASTKD5 line 2: V3SH11252-228281042) or *PRDX3* (sh-PRDX3 line 1: V3SH11252-224976620 and sh-PRDX3 line 2: V3SH11252-224980877) were purchased from Horizon Discovery. Lentiviruses were made by co-transfection of the lentiviral vector, VSV-G and ΔNRF into HEK293T cells. Jurkat cells were infected with lentiviruses containing shRNA by spinoculation (1,000*g* at 25 °C for 3 h) to generate relevant knockdown cell lines. Silencing of *FASTKD5* and *PRDX3* was induced by 1 μg ml^{-1} doxycycline (D3447, Sigma-Aldrich) for 72 h. To double knock down *NLRX1* and *FASTKD5*, Jurkat-sh-NLRX1 line 2 cells were transduced with sh-FASTKD5 line 1. To reduce *NLRX1* expression in human primary CD4$^+$ T cells, cells were stimulated with anti-CD3/anti-CD28-coated magnetic beads for 24 h and then transduced with concentrated lentiviruses expressing sh-NLRX1 (MOI = 5). Beads were removed at day 5 after stimulation. Transduced CD4$^+$ T cells were expanded in a complete RPMI medium containing 200 IU ml^{-1} of interleukin-2.

Luciferase assay. Various Jurkat cell lines were seeded in U-bottom 96-well plates at a density of 1.0×10^5 per well and infected with VSV-G-NL4-3-Luc at the MOI as indicated in figure legends. At indicated time points, cells were collected and measured for firefly luciferase activity by the Luciferase Assay Reagent II (Promega) according to the manufacturer's instruction. Total proteins were quantified by the Pierce BCA Protein Assay kit. Luciferase activity was normalized by 1 μg of total proteins.

Immunoblotting. Jurkat cells infected with HIV pseudoviruses or lentiviruses as indicated in figure legends were collected and subjected to immunoblot as previously described[14]. Primary antibodies included anti-NLRX1 (generated by Ting laboratory, 1:2,000 dilution), anti-HIV-1 p24 (39/5.4A, 1:500 dilution), anti-STAT1 (9172, 1:1,00 dilution), anti-phospho-STAT1 (Y701, 9171, 1:1,000 dilution; Cell Signaling Technology), anti-FASTKD5 (ab111548, 1:1,000 dilution), anti-PRDX3 (ab73349, 1:1,000 dilution), anti-SPNS1 (ab59971, 1:1,000 dilution; Abcam) and anti-β-actin (sc-1615, HRP conjugate, 1:5,000 dilution; Santa Cruz Biotechnology). Appropriate HRP-conjugated secondary antibodies were used and proteins were detected using Enhanced Chemiluminescent reagent (Thermo Fisher Scientific). Densitometry analysis was performed for Gag p55 levels by normalizing to β-actin using ImageJ (NIH).

Measurement of HIV-1 replication by flow cytometry. Jurkat cells and human primary CD4$^+$ T cells infected with HIV-1 R3A were collected at 48 hpi and fixed and permeabilized using Fixation/Permeabilization Solution kit (BD Biosciences) according to manufacturer's instructions, followed by intracellular staining with anti-HIV-1 p24-FITC for 30 min. HIV-1 p24-positive cells were determined using a CyAn ADP flow cytometer. Summit v.5.0 was used for sample collection and FlowJo v.9 was used for data analysis.

Measurement of NLRX1 expression by imaging flow cytometry. Jurkat cells were infected with VSV-G-NL4-3-EGFP (MOI = 0.5). At 48 hpi, cells were fixed and permeabilized using Fixation/Permeabilization Solution kit. Intracellular staining of NLRX1 was conducted using 1 μg ml^{-1} anti-NLRX1 (PA5-21018, Invitrogen) and then 1 μg ml^{-1} Alexa Fluor 647 donkey anti-rabbit IgG (406414, BioLegend) for 30 min on ice, respectively. After staining, images of cells expressing GFP and NLRX1 were obtained by ImageStreamX MkII (Luminex Corporation). Data were analyzed by IDEAS6.2 software.

Human CD4$^+$ T cell-reconstituted mouse model for HIV-1 infection. To test the efficacy of NLRX1 silencing in HIV-1 infection using an in vivo model, total CD4$^+$ T cells isolated from one healthy donor were activated and transduced by lentiviruses to generate *NLRX1*-silenced cells as described above. NRG mice (007799, Jackson Laboratory) bred and housed in specific-pathogen-free conditions at 19–23 °C with a 12-h-light–dark cycle were irradiated as previously described[24]. Mice at 4–6 weeks of age were randomly assigned to four groups ($n = 4$ for each uninfected group and $n = 5$ for each infected group) to control for sex and age effects. On the day of transfusion, 1.0×10^7 human CD4$^+$ T cells transduced with lentiviruses expressing sh-Ctr or sh-NLRX1 in 100 μl PBS were injected into each mouse via the tail vein to generate human CD4$^+$ T cell-reconstituted mice (NRG-hu CD4$^+$). The day after, each mouse was infected with 1 ng p24 HIV-1 R3A via the retro-orbital route. Blood was collected weekly after infection through the tail, with plasma and cell pellets separated by centrifugation at 5,000 r.p.m. for 5 min and plasma was stored at −80 °C for further viral RNA extraction. For VL determination, viral RNA extracted from standard plasma (3443, NIH AIDS Reagent Program) and plasma from each infected mouse (QIAamp viral RNA minikit, QIAGEN) was analyzed by quantitative PCR with reverse transcription (RT–qPCR) (TaqMan One-Step RT–qPCR master mix, Applied Biosystems). The primers and probe used here were the same as those used to quantify HIV-1 replication described above. Cell pellets were used to quantify human CD4$^+$ T cells. Briefly, red blood cells were lysed using ammonium-chloride-potassium (ACK) lysis buffer (A1049201, Gibco) at room temperature for 5 min. Cells were then resuspended in FACS buffer (PBS containing 2% FBS) and stained for cell viability (7-aminoactinomycin D, A1310, Life Technologies) and surface markers, including mouse CD45 (PE-Cy5-conjugated, clone 30-F11, BioLegend, 1:330 dilution), human CD3 (PE-conjugated, clone HIT3a, BioLegend, 1:330 dilution) and human CD4$^+$ (FITC-conjugated, RPA-T4, BioLegend, 1:330 dilution). After staining, cell populations were analyzed by flow cytometry analysis using the CyAn ADP flow cytometer. Stained cells were counted by using a Guava easyCyte flow

cytometer (Millipore). After 3 wpi, spleens were isolated after mice were killed and splenocytes were counted using a Guava easyCyte flow cytometer after staining of live/dead cells.

For in vivo testing of metformin in HIV-1 replication, NRG-hu CD4$^+$ mice were administered metformin by drinking water (5 mg ml^{-1}) 1 d before infection and during the whole infection period. The water bottles containing freshly made metformin solution were changed every 3–4 d. Viremia and human CD4$^+$ T cell counts were determined as described above.

Immunoprecipitation. Jurkat-sh-Ctr or Jurkat-sh-NLRX1 cells (5×10^7) were washed twice by PBS and then resuspended in 1 ml lysis buffer (50 mM Tris, 150 mM NaCl, 1% Triton X-100, protease inhibitor cocktail, phosphatase inhibitor cocktail, pH 7.4). Cell lysates were rotated at 4 °C for 30 min to obtain complete cell lysis and cell debris was pelleted by centrifugation at 16,000*g* for 30 min at 4 °C. Partially cleared lysates (80 µl) were kept for use as the input for immunoblotting. Immunoprecipitation was performed by incubating cell lysates with 10 µg anti-NLRX1 or control mouse IgG1 antibody (5415, Cell Signaling) plus 50 µl protein A/G-conjugated agarose beads (53133, Thermo Fisher Scientific) for 8 h, followed by washing three times with lysis buffer. Proteins pulled down by antibodies were subjected to immunoblotting with antibodies specific for NLRX1, FASTKD5, PRDX3 and SPNS1. To determine the interaction of NLRX1 and FASTKD5 upon HIV-1 infection, 1×10^8 Jurkat cells were infected with 100 ng p24 HIV-1 R3A. At 72 hpi, immunoprecipitation and immunoblotting were conducted as described above.

Metabolism assays. Jurkat cells containing various shRNAs were infected with VSV-G-NL4-3-Luc (MOI = 3) or left uninfected. For drug treatment, 5 mM metformin was maintained in cell cultures through virus infection and metabolic assays; 5 µM resveratrol was added in the cell culture during infection but was removed during metabolic assays. At 24 hpi, each group was plated in quintuplicate in the Seahorse XF24 Cell Culture Microplates (Agilent) (1×10^6 per well) with 500 µl Seahorse XF base medium (Agilent), 100 mM sodium pyruvate (11360070, Gibco) and 2.5 M glucose (A2494001, Gibco) for OCR measurements, and with 500 µl Seahorse XF base medium with 100 mM sodium pyruvate and 2 mM glutamine (25030081, Gibco) for ECAR measurements for 1 h in the absence of CO_2 at 37 °C before the start of the metabolism assay. OCR and ECAR were assessed as previously described[46]. In some experiments, OCR and ECAR were normalized to the basal levels initially recorded. The following parameters were assessed as indices of mitochondrial respiratory function: basal respiration (difference between basal and rotenone-induced OCR), maximal respiration (difference between FCCP-induced and rotenone-induced OCR) and reserved respiratory capacity (difference between maximal and basal respiration). Glycolytic flux activation was determined by levels of glycolysis (ECAR in response to glucose), glycolytic capacity (maximal ECAR following oligomycin exposure) and glycolytic reserve (difference between 2-DG-induced and oligomycin-induced ECAR).

Quantitative proteomics analysis. Stable isotope labeling by amino acids in cell culture (SILAC)-based quantitative proteomics has been previously described[47]. Five million SILAC-labeled Jurkat-sh-Ctr or Jurkat-sh-NLRX1 cells were infected with VSV-G-NL4-3-Luc (MOI = 5) or left uninfected. At 24 hpi, cells were collected and subjected to mass spectrometry. For TMT-based quantitative proteomics, 5×10^6 Jurkat cells expressing sh-FASTKD5 or control cells were infected with VSV-G-NL4-3-Luc (MOI = 5) or left uninfected. At 24 hpi, cells were collected and cell pellets were resuspended in 8 M Urea, 50 mM Tris-HCl (pH 8.0), reduced with 5 mM dithiothreitol for 30 min at room temperature and alkylated with 15 mM iodoacetamide for 45 min in the dark at room temperature. Samples were diluted fourfold with 25 mM Tris-HCl (pH 8.0), 1 mM $CaCl_2$ and digested with trypsin at 1:100 (*w*/*w*, trypsin:protein) ratio overnight at room temperature. Peptides were desalted on homemade C18 stagetips. Then, 100 µg of each peptide sample was labeled with TMT11plex Isobaric Label Reagent (A34808, Thermo Fisher Scientific) following the optimal protocol[48]. The mixture of labeled peptides was desalted and fractionated into 24 fractions in 10 mM trimethylammonium bicarbonate buffer containing 5–40% acetonitrile. For mass spectrometry analysis, dried peptides were dissolved in 0.1% formic acid and 2% acetonitrile. For global profiling samples, peptide concentration was measured with Pierce Quantitative Colorimetric Peptide Assay (23275, Thermo Fisher Scientific). Then, 0.5 µg of each fraction was analyzed on a Q-Exactive HF-X coupled with an Easy nanoLC 1200 (Thermo Fisher Scientific). Peptides were loaded on to a nanoEase MZ HSS T3 Column (100 Å, 1.8 µm, 75 µm × 150 mm, Waters). Analytical separation of all peptides was achieved with a 100-min gradient. A linear gradient of 5–10% buffer B over 5 min, 10–31% buffer B over 70 min and 31–75% buffer B over 15 min was executed at a 300 nl min^{-1} flow rate followed by a ramp to 100% B in 1 min and a 9-min wash with 100% B (where buffer A was aqueous 0.1% formic acid and buffer B was 80% acetonitrile and 0.1% formic acid). liquid chromatography–mass spectrometry (MS) experiments were also carried out in a data-dependent mode with full MS (externally calibrated to a mass accuracy of <5 ppm and a resolution of 120,000 for TMT-labeled samples at *m*/*z* 200) followed by high-energy collision-activated dissociation MS/MS with a resolution of 45,000 for TMT-labeled global samples at *m*/*z* 200. High-energy collision-activated dissociation MS/MS was used to dissociate peptides at a normalized collision energy of 32 eV (for TMT-labeled samples) in the presence of nitrogen bath gas atoms. Dynamic exclusion was 45 or 20 s. For raw proteomics data processing and analysis, mass spectra were processed and peptide identification was performed using MaxQuant software v.1.6.10.43 (Max Planck Institute). All protein database searches were performed against the UniProt human protein sequence database (UP000005640). An FDR for both peptide-spectrum match and protein assignment was set at 1%. Search parameters included up to two missed cleavages at Lys/Arg on the sequence, oxidation of methionine and protein N-terminal acetylation as a dynamic modification. Carbamidomethylation of cysteine residues was considered as a static modification. Peptide identification was performed by filtering reverse and contaminant entries and assigning them to their leading razor protein. The TMT reporter intensity found in MaxQuant was used for quantitation. Data processing and statistical analysis were performed on Perseus (v.1.6.10.50). Protein quantitation was performed using TMT reporter intensity and a two-sample Student's *t*-test statistics on two biological replicates was used with a *P* value of 5% to report statistically significant protein abundance fold changes. Functional analysis was performed by ingenuity pathway analysis (QIAGEN), ReactomeFIplugin in Cytoscape and Metascape. Heat maps were generated by Morpheus. The Venn diagram was generated through https://www.meta-chart.com.

Analysis of RV217 transcriptome data. For microarray analysis, the LIMMA package was used to fit a linear model and calculate the association of gene expression to the magnitude of set-point viremia[49]. For pathway analysis, GSEA using the KEGG database was performed to identify pathway-associated set-point VL or *NLRX1* expression[50]. GSEA is a statistical method to determine whether members of a particular gene set preferentially occur toward the top or bottom of a ranked-ordered gene list, where genes are ranked by the strength of their association with the outcome of interest (set-point VL). More specifically, GSEA calculates a NES that reflects the degree to which a set of genes is overrepresented among genes differentially expressed along with set-point VL. The significance of an observed NES was obtained by permutation testing: re-sorting the gene list to determine how often an observed NES occurs by chance. An analysis for the association of gene expression to *NLRX1* expression level was also performed by using the LIMMA package and GSEA similar to the above description. Leading-edge analysis was performed to examine the particular genes of a gene set contributing the most to the enrichment. For network mapping/visualization, GeneMANIA Networks (Genemania.org) were plotted to represent coexpression of leading-edge genes of the OXPHOS pathway[51]. The overlap between the genes included in the networks and Gene Ontology biological process was assessed using a Fisher's exact test. GeneMANIA is a flexible, user-friendly web interface for generating hypotheses about gene functions, analyzing gene lists and prioritizing genes for functional assays. Given a query list, GeneMANIA extends the list with functionally similar genes that it identifies using available genomics and proteomics data. GeneMANIA also reports weights that indicate the predictive value of each selected dataset for the query. The Cytoscape (cytoscape.org) plugin was used to plot networks. An alternative network for leading-edge genes of the OXPHOS pathway was generated by ClueGO or STRING v.11.

Statistical analysis. Statistical significance was assessed by unpaired Student's *t*-test or ANOVA followed by Dunnett's, Šidák's or Tukey's multiple comparisons test in GraphPad Prism 8.4.3 software, Wilcoxon rank-sum test or Pearson correlation. In all tests, *P* values were shown in the figures.

Reporting Summary. Further information on research design is available in the Nature Research Reporting Summary linked to this article.

Data availability

The authors declare that the data supporting the findings of this study are available with the paper and its supplementary information files. Source data for all figures are provided with the paper. The RV217 CD4$^+$ T cell transcriptome data have been uploaded to the Gene Expression Omnibus (accession number GSE165841). The mass spectrometry proteomics data have been deposited to the ProteomeXchange with identifier PXD023565. The public databases used include UniProt human protein sequence database https://www.uniprot.org/proteomes/UP000005640; KEGG pathway database https://www.genome.jp/kegg/pathway.html; Hallmark gene set https://www.gsea-msigdb.org/gsea/msigdb/genesets.jsp?collection=H; and Reactome Pathway database https://reactome.org/. Source data are provided with this paper.

References

42. Committee for the Update of the Guide for the Care and Use of Laboratory Animals et al. *Guide for the Care and Use of Laboratory Animals* 8th edn (National Academies Press, 2011).
43. Konig, R. et al. Global analysis of host-pathogen interactions that regulate early-stage HIV-1 replication. *Cell* **135**, 49–60 (2008).

44. Guo, H., Gao, J., Taxman, D. J., Ting, J. P. & Su, L. HIV-1 infection induces interleukin-1β production via TLR8 protein-dependent and NLRP3 inflammasome mechanisms in human monocytes. *J. Biol. Chem.* **289**, 21716–21726 (2014).
45. Livak, K. J. & Schmittgen, T. D. Analysis of relative gene expression data using real-time quantitative PCR and the $2^{-\Delta\Delta C_T}$ method. *Methods* **25**, 402–408 (2001).
46. Uchimura, T. et al. The innate immune sensor NLRC3 acts as a rheostat that fine-tunes T cell responses in infection and autoimmunity. *Immunity* **49**, 1049–1061 (2018).
47. Chen, X., Smith, L. M. & Bradbury, E. M. Site-specific mass tagging with stable isotopes in proteins for accurate and efficient protein identification. *Anal. Chem.* **72**, 1134–1143 (2000).
48. Zecha, J. et al. TMT labeling for the masses: a robust and cost-efficient, in-solution labeling approach. *Mol. Cell Proteom.* **18**, 1468–1478 (2019).
49. Smyth, G. K. et al. in *Bioinformatics and Computational Biology Solutions using R and Bioconductor* 1st edn (eds. Gentleman, R., Carey, V., Huber, W., Irizarry, R. & Dudoit, S.) 379–420 (NY Springer, 2005).
50. Subramanian, A. et al. Gene set enrichment analysis: a knowledge-based approach for interpreting genome-wide expression profiles. *Proc. Natl Acad. Sci. USA* **102**, 15545–15550 (2005).
51. Mostafavi, S., Ray, D., Warde-Farley, D., Grouios, C. & Morris, Q. GeneMANIA: a real-time multiple association network integration algorithm for predicting gene function. *Genome Biol.* **9**, S4 (2008).

Acknowledgements

We thank the UNC Flow Cytometry Core Facility, supported in part by P30 CA016086 Cancer Center Core Support Grant to the UNC Lineberger Comprehensive Cancer Center, for assistance with flow cytometry. We thank S. K. Chanda at Sanford Burnham Prebys Medical Discovery Institute for providing the pNL4-3.EGFP.E- construct. This work was supported by NIH grants R01-AI029564 (J.P.-Y.T.), U19AI109965 (J.P.-Y.T.), AI127346 (L.S.) and DK119937 (L.S.); and UNC CFAR Award P30 AI50410 (H.G.). The RV217 study was supported by a cooperative agreement (W81XWH-18-2-0040) between the Henry M. Jackson Foundation for the Advancement of Military Medicine and the US Department of Defense.

Author contributions

H.G., L.S. and J.P.-Y.T. designed the experiments; H.G., Q.W., L.W., K.G., E.R., E.H.G., L.C., M.L.R. and L.A.E. conducted the studies; K.G. performed the data and statistical analyses of the RV217 study. X.C. and R.-P.S. assisted with the experiments and provided intellectual input; D.M.M. and C.G. provided critical reagents; J.P.-Y.T. supervised the study; H.G., Q.W., L.S. and J.P.-Y.T. interpreted the data and wrote the manuscript.

Competing interests

The authors declare no competing interests. The views expressed are those of the authors and should not be construed to represent the positions of the US Army, the Department of Defense or the Henry M. Jackson Foundation.

Additional information

Extended data is available for this paper at https://doi.org/10.1038/s41590-021-00898-1.

Supplementary information The online version contains supplementary material available at https://doi.org/10.1038/s41590-021-00898-1.

Correspondence and requests for materials should be addressed to L.S. or J.P.-Y.T.

Peer review information *Nature Immunology* thanks Xiao-Ning Xu and the other, anonymous, reviewer(s) for their contribution to the peer review of this work. Peer reviewer reports are available. Zoltan Fehervari was the primary editor on this article and managed its editorial process and peer review in collaboration with the rest of the editorial team.

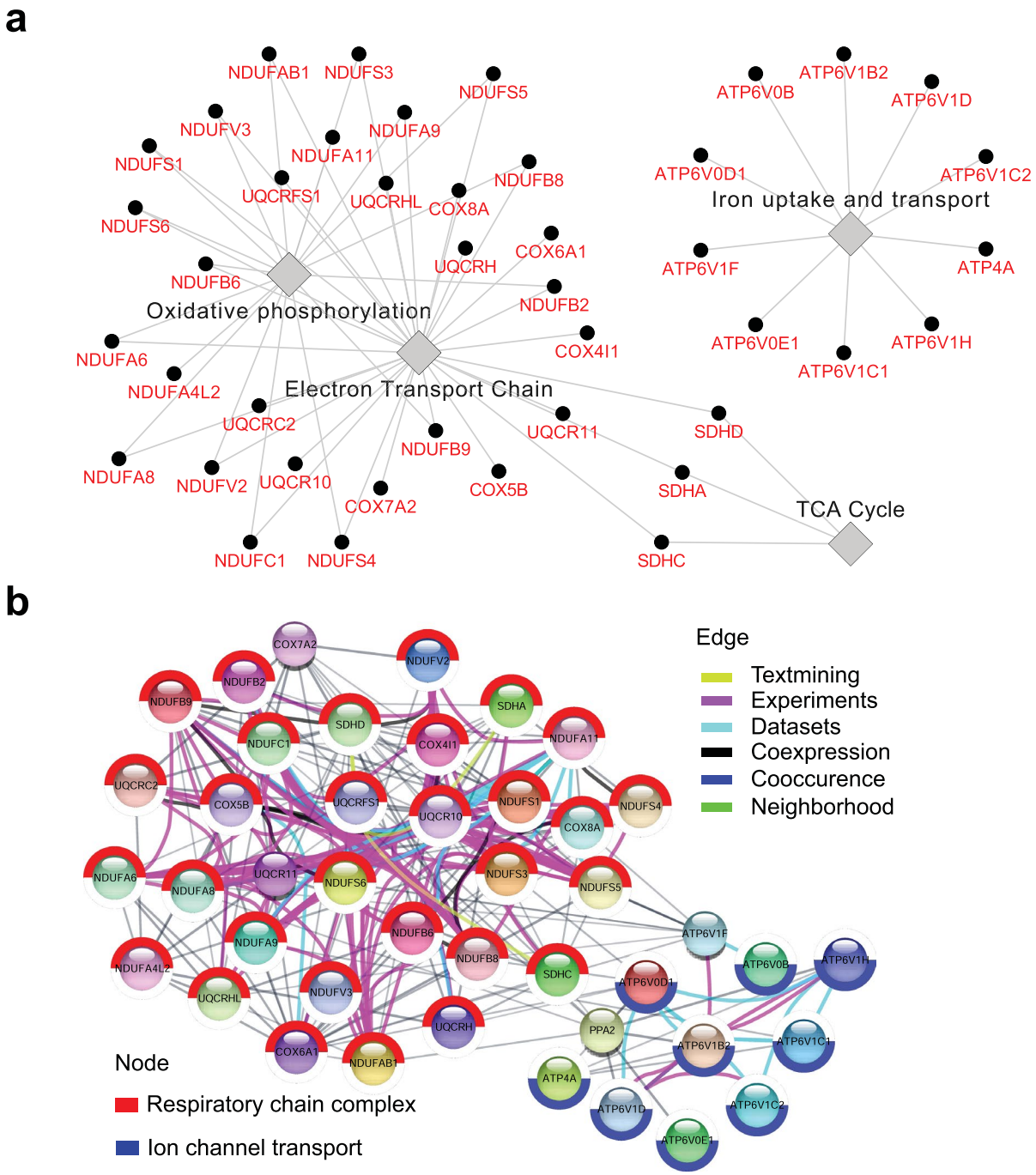

Extended Data Fig. 1 | The network of leading edge genes in the OXPHOS pathway associated with set-point viral load. a, Cytoscape was used to plot a network highlighting the top genes contributing to enrichment. The ClueGO app was used to infer network connections. Nodes represent genes, and edges reflect the association between these genes. **b**, STRING was used to plot a network highlighting the top genes contributing to enrichment. Nodes represent genes, and edges reflect the association between these genes.

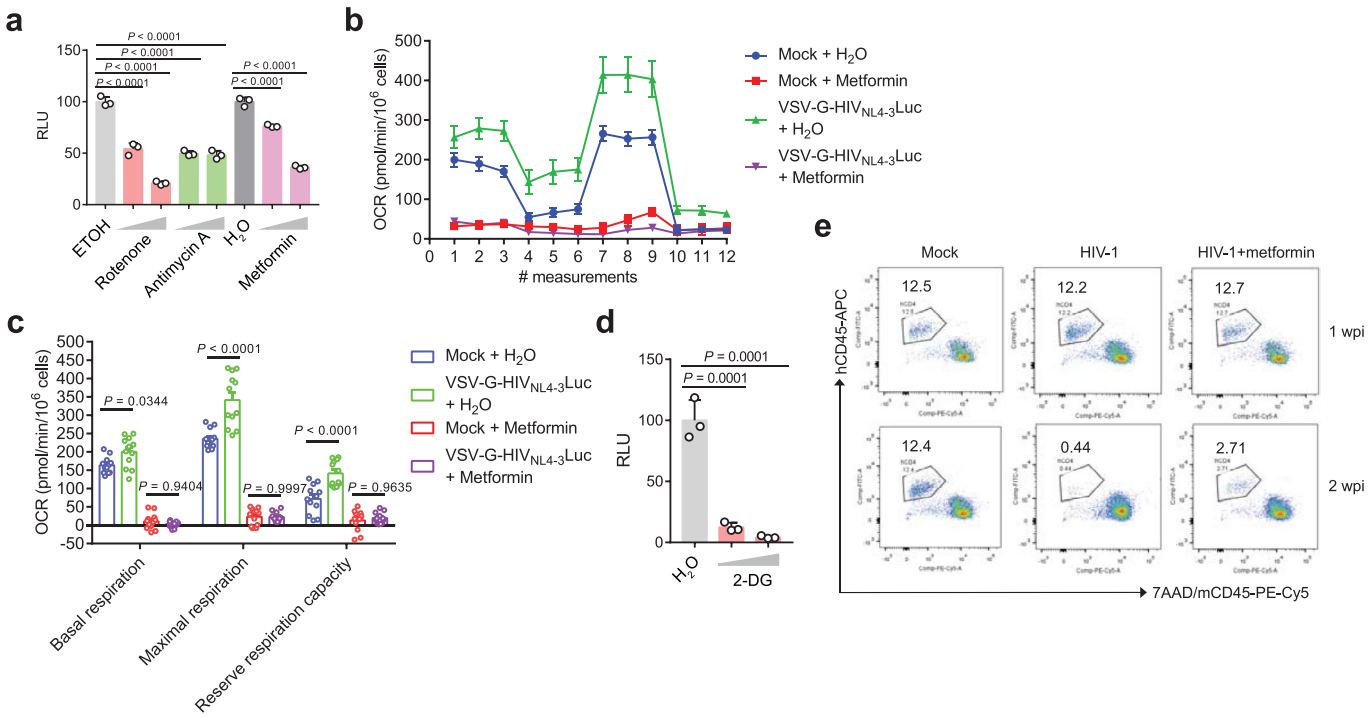

Extended Data Fig. 2 | Metabolic inhibitors suppress HIV-1 replication in CD4 T cells and NRG-hu CD4 mice. a, The effect of OXPHOS inhibitors on virus replication in VSV-G-NL4-3-Luc-infected Jurkat cells. Rotenone (0.2 μM or 1 μM), metformin (1 mM or 5 mM, mitochondrial complex I inhibitor) and antimycin A (0.2 μM or 1 μM, mitochondrial complex III inhibitor). Ethanol is the vehicle control for rotenone and antimycin A, and sterile water is the vehicle control for metformin. n = 3 cell cultures per experiment. **b**, The oxygen consumption rate (OCR) was measured in Jurkat cells infected with VSV-G-NL4-3-Luc or left uninfected (mock) in the presence of metformin or the vehicle control (H2O). n = 4 cell cultures per experiment. **c**, The basal and maximal OCR and reserved respiratory capacity of Jurkat cells infected with VSV-G-NL4-3-Luc or left uninfected (mock) in the presence of metformin or vehicle control (H2O). n = 12 cell cultures per experiment. **d**, The effect of 2-DG (5 mM or 10 mM), a glycolysis inhibitor, on virus replication in VSV-G-NL4-3-Luc infected Jurkat cells. H2O was used as vehicle control. n = 3 cell cultures per experiment. **e**, Representative FACS plots of human CD4 T cells from peripheral blood stained with the indicated markers. Cells were obtained from mock or HIV-1 R3A infected NRG-hu CD4 mice with or without metformin treatment. Data are representative of three independent experiments shown as the mean ± s.e.m. Statistical significance was tested by one-way ANOVA (**a**,**d**) or two-way ANOVA followed by Tukey's multiple comparisons test (**c**).

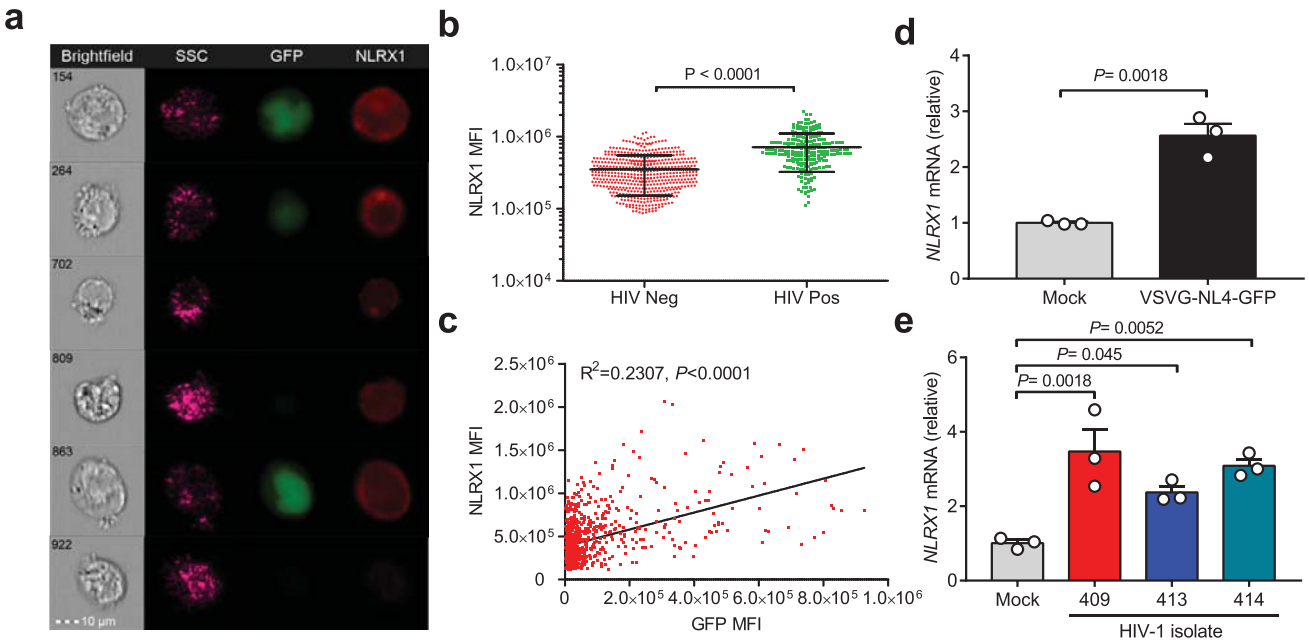

Extended Data Fig. 3 | NLRX1 is upregulated in HIV-1 infected CD4 T cells. a, Jurkat cells were infected with VSV-G-pseudotyped HIV NL4-3-EGFP virus (MOI = 0.5). After 48 hours post-infection (hpi), cells were stained with an anti-NLRX1 antibody and subjected to ImageStreamX MkII imaging flow cytometry. GFP positive cells indicate HIV-1 infection. **b**, The mean fluorescence intensity (MFI) of NLRX1 staining in GFP negative (n = 532 cells) and positive cells (n = 222 cells). *P* value was calculated by two-tailed unpaired Student's *t*-test. **c**, The linear relationship between the expression of *NLRX1* and GFP. *R*, Pearson's correlation coefficient; Correlation is significant at $P < 0.0001$. **d**, Jurkat cells were infected by VSV-G-NL4-3-EGFP pseudovirus (MOI = 1). At 48 hpi, *NLRX1* transcripts were assessed by qPCR. n = 3 cell cultures per experiment. *P* value was calculated by two-tailed unpaired Student's t-test. **e**, *NLRX1* transcripts were assessed in human primary CD4 T cells infected by three different HIV-1 clinical isolates at 48 hpi by qPCR. n = 3 cell cultures per experiment. Significance was tested by one-way ANOVA followed by Dunnett's multiple comparisons test. All data are representative of three independent experiments. Error bar is s.e.m.

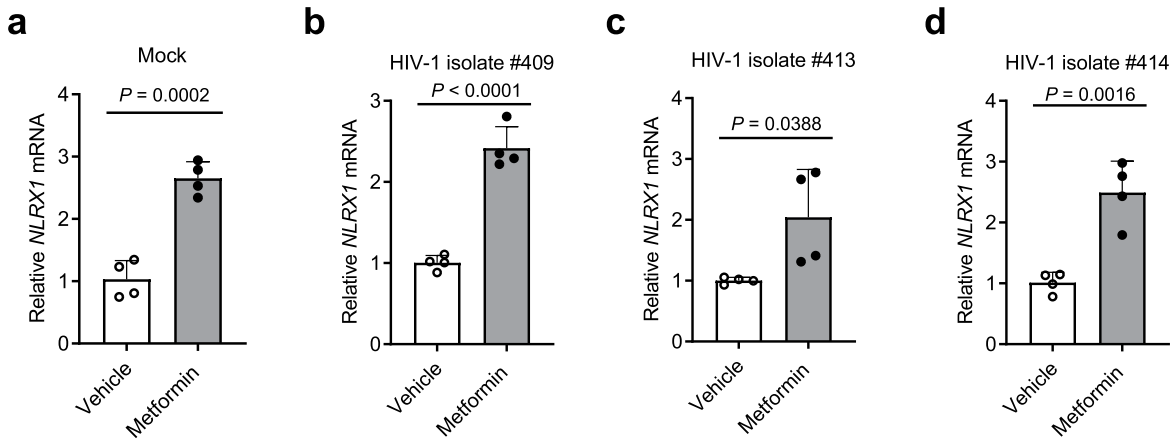

Extended Data Fig. 4 | The effect of metformin on NLRX1 expression in CD4 T cells. a–d, CD3/CD28 antibody-activated human primary CD4 T cells were left uninfected (**a**) or infected by three different HIV-1 clinical isolates, #409 (**b**), #413 (**c**), and #414 (**d**) in the presence of 5 mM metformin or the vehicle control, sterile water. *NLRX1* transcripts were assessed at 48 hpi by qPCR. Representative data of three independent experiments are shown as the mean ± standard deviation (s.d). n = 4 cell cultures per experiment. Statistical significance was tested by two-tailed unpaired Student's *t*-test.

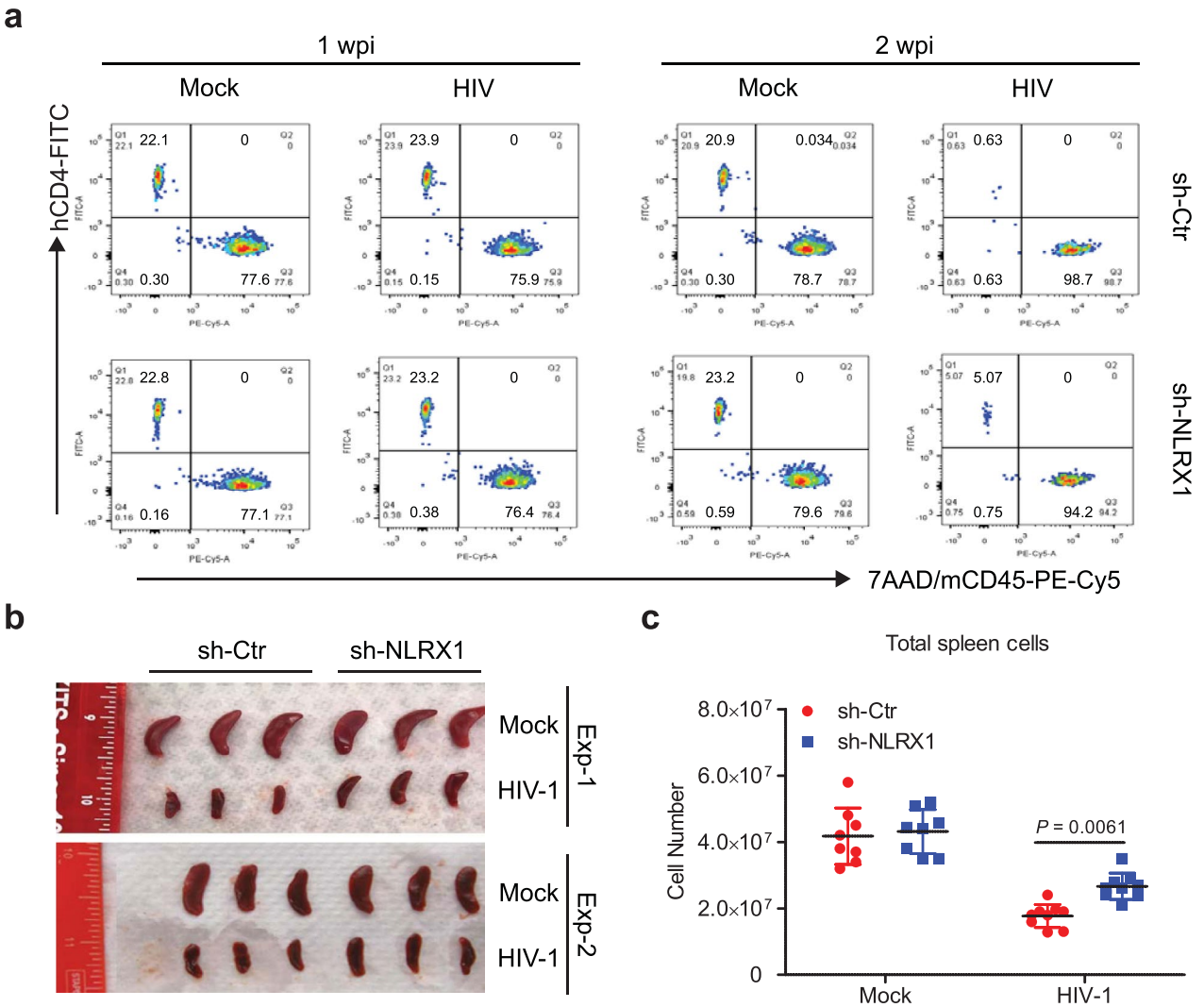

Extended Data Fig. 5 | Silencing NLRX1 protects HIV-1 caused human CD4 T cell depletion in the NRG-hu CD4 mouse model. a, Representative fluorescence-activated cell sorting (FACS) plot of human CD4 T cells expressing the indicated markers in peripheral blood from mock or HIV-1 R3A infected NRG-hu CD4 mice at 1 and 2 wpi. **b**, Spleens from mock or HIV-1 R3A infected NRG-hu CD4 mice at 3 wpi. n = 6 mice per group. **c**, Splenocyte numbers of mock or HIV-1 R3A infected NRG-hu CD4 mice at 3 wpi. The data are a pool of two independent experiments. n = 8 mice for mock groups; n = 9 mice for HIV-1 infection groups. Data are presented as the mean ± s.e.m. Statistical significance was tested by two-way ANOVA followed by Sidak's multiple comparisons test.

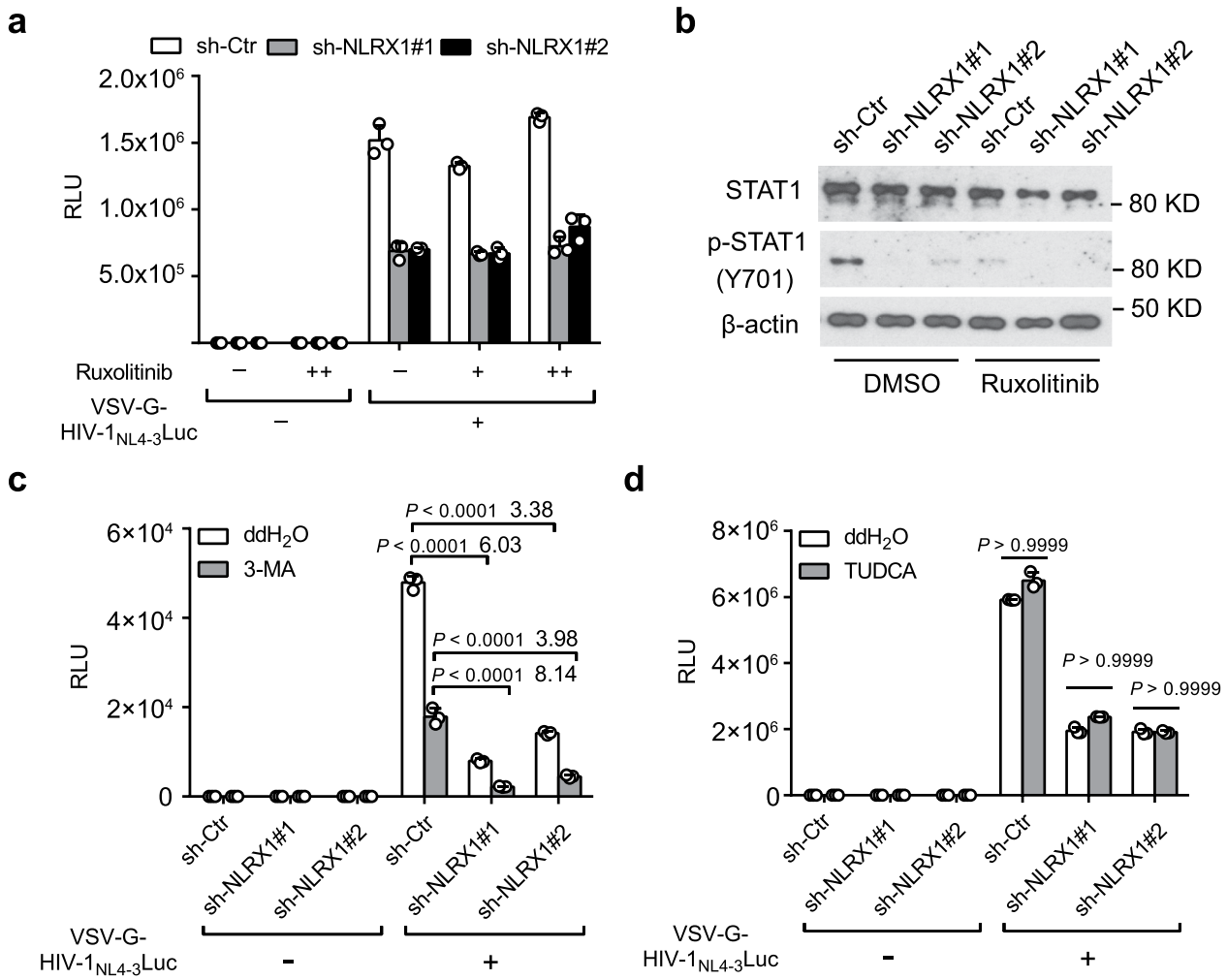

Extended Data Fig. 6 | NLRX1 promotion of HIV-1 replication in CD4 T cells is independent of IFN-I, autophagy, or ER stress. a, RLU in Jurkat sh-Ctr or sh-NLRX1 cells infected with VSV-G-NL4-3-Luc (MOI=1) or left uninfected in the presence or absence of JAK1/2 inhibitor Ruxolitinib at 24 hpi. n = 3 cell cultures per experiment. **b**, Ruxolitinib suppressed VSV-G-NL4-3-Luc infection-induced phosphorylation of STAT1 at 24 hpi. β-actin was used as the loading control. **c**, Similar to **a** except for using autophagy inhibitor 3-Methyladenine (3-MA) to treat cells. Numbers on top of the bar are the fold differences. n = 3 cell cultures per experiment. **d**, Similar to **a** except for using ER stress inhibitor sodium tauroursodeoxycholate (TUDCA) to treat cells. Luciferase activities were determined at 48 hpi. n = 3 cell cultures per experiment. Representative data of three independent experiments are presented as the mean ± s.e.m. Two-way ANOVA followed by Sidak's multiple comparisons test.

a

Bait	Hit	Localization	Go - Biological process
NLRX1	CDIPT	plasma membrane and ER	CDP-diacylglycerol metabolic process, phosphatidylinositol biosynthetic process
	FASTKD5	mitochondrial	Cellular respiration, mitochondria mRNA processing, mRNA processing
	HAUS6	Cytoplasm, Cytoskeleton, Microtubule	Cell division, G2/M transition of mitotic cell cycle
	PRDX3	mitochondrial	cell redox homeostasis, cellular response to oxidative stress, positive regulation of cell proliferation, regulation of mitochondrial membrane potential
	SPNS1	Mitochondrion inner membrane	lipid transport, transmembrane transport

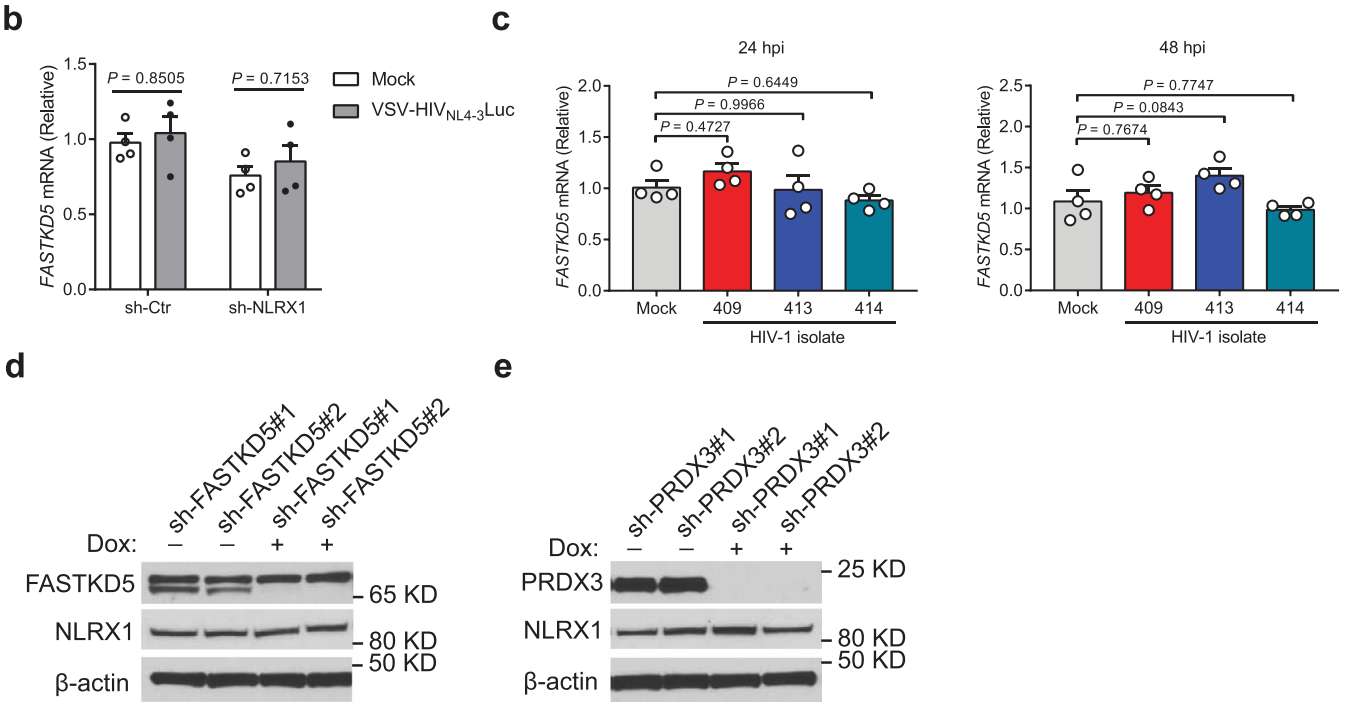

Extended Data Fig. 7 | Expression of *FASTKD5* in Jurkat cells and primary human CD4 T cells. a, Candidates of NLRX1 interacting proteins identified by immunoprecipitation (IP)-mass spectrometry (MS) using overexpressed NLRX1 as the bait in a previous publication. **b**, Jurkat-sh-Ctr and Jurkat-sh-NLRX1 cells were left uninfected (mock) or infected by VSV-G-NL4-3-Luc pseudovirus (MOI = 1). *FASTKD5* transcripts were assessed at 24 hpi by qPCR. Data are shown as the mean ± s.e.m. n = 4 cell cultures per experiment. Statistical significance was tested by two-way ANOVA followed by Sidak's multiple comparisons test. **c**, CD3/CD28 antibody-activated human primary CD4 T cells were infected by three different HIV-1 clinical isolates (10 ng p24), and *FASTKD5* transcripts were assessed at 24 and 48 hpi by qPCR. Data are shown as the mean ± s.e.m. n = 4 cell cultures per experiment. Statistical significance was tested by one-way ANOVA followed by Dunnett's multiple comparisons test. **d**, **e**, Doxycycline-induced silencing of FASTKD5 (**d**) and PRDX3 (**e**) in Jurkat cells transduced by 2 different shRNA containing lentiviruses. β-actin was used as the loading control. Data (**b**–**e**) are representative of three independent experiments.